REPORT DOCUMENTATION PAGE

AFRL-SR-AR-TR-03-

-0152

1. AGENCY USE ONLY *(Leave blank)*

2. REPORT DATE
14 MARCH 2003

3. REPORT TYPE AND DATES COVERED
FINAL REPORT 1 AUG 00 TO 31 JAN 03

4. TITLE AND SUBTITLE
SINGLE-MODE WAVELENGTH DIVISION DEMULTIPLEXER FOR BIT-PARALLEL FIBER OPTIC NETWORKS

5. FUNDING NUMBERS
F49620-00-C-0026

1660/01

62173C

6. AUTHOR(S)
DR JIE QIAO, PROJECT MANAGER
DR BIPIN BIHARI, SENIOR SCIENTIST
DR RAY T. CHEN, CONSULTANT

7. PERFORMING ORGANIZATION NAME(S) AND ADDRESS(ES)
OMEGA OPTICS, INC.
13010 RESEARCH BLVD. SUITE 216
AUSTIN, TX 78750

8. PERFORMING ORGANIZATION REPORT NUMBER

9. SPONSORING/MONITORING AGENCY NAME(S) AND ADDRESS(ES)
AFOSR/NL
4015 WILSON BLV. SUITE 713
ARLINGTON, VA 22203-1954

10. SPONSORING/MONITORING AGENCY REPORT NUMBER

11. SUPPLEMENTARY NOTES

12a. DISTRIBUTION AVAILABILITY STATEMENT
APPROVE FOR PUBLIC RELEASE: DISTRIBUTION UNLIMITED

12b. DISTRIBUTION CODE

20030513 079

13. ABSTRACT *(Maximum 200 words)*

In summary, this SBIR program was highly successful, and a few modules were completely packaged for delivery to the JPL labs for further testing. We contacted the JPL team at a later stage. However, it appears that JPL team was not interested in taking delivery of these modules. However, a set of 32-channel WDM/WDDM modules were successfully used to demonstrate a high throughput bit-serial data transfers between two computers for another program. The main achievements of this program are: 1) The specifications, and finalized the device structure of the WDDM for bit-parallel computer architecture have been established. 2) A bulk ruled reflection high-order Echelle grating was employed to realize high dispersion, to achieve high diffraction efficiency within a wide spectral range, and low polarization dependent loss. A diffraction limited triplet lens was designed to serve for both of collimation and focusing simultaneously, so the device cost and size were decreased dramatically. 3) We also designed a 33-channel fiber array with non-uniform channel spacing to compensate the non-linear effect of angular dispersion. 4) Graded index lensed fibers were designed and fabricated to expanc the mode field diameter, and then to increase passband and alignment tolerance. 5) A thorough thermal analysis and optimization has been performed to achieve athermalized
WDM design and packaging. 6) In order to further broaden the passband to meet the specification, a 40 channel. 7) 100 GHz interleaver-based DWDM were designed and a prototype was built.

14. SUBJECT TERMS

15. NUMBER OF PAGES

16. PRICE CODE

17. SECURITY CLASSIFICATION OF REPORT	18. SECURITY CLASSIFICATION OF THIS PAGE	19. SECURITY CLASSIFICATION OF ABSTRACT	20. LIMITATION OF ABSTRACT
UNCLAS	UNCLAS	UNCLAS	

OMEGA OPTICS INC.

SINGLE-MODE WAVELENGTH DIVISION DEMULTIPLEXER FOR BIT-PARALLEL FIBER OPTIC NETWORKS

SBIR Contract No.: F49620-00-C-0026

March 14, 2003

Final Report

Authors

Dr. Jie Qiao, Project Manager

Dr. Bipin Bihari, Senior Scientist

Dr. Ray T. Chen, Consultant

Contractual point of contact:

Mr. Kenneth Chen, President

Phone: 512-996-8833

Fax: 512-335-9681

E-mail: *Kenneth.chen@eomegaoptics.com*

Table of Contents

Table of Figures

List of Tables

1.0 EXECUTIVE SUMMARY

Wavelength-division multiplexing (WDM) technology, by which multiple optical channels can be simultaneously transmitted at different wavelengths through a single optical fiber, is a useful means of making full use of the low-loss characteristics of optical fibers over a wide-wavelength region. Besides its capability to efficiently exploit the huge bandwidth of single mode optical fibers, WDM is promising for constructing different levels of transparency to optical transmissions (i.e., independent of data bit-rate, modulation format, or protocol), which permits excellent upgrading and backward compatibility of the current networks. This makes WDM the key technology for tomorrow's developments in data, voice, imaging, and video communications.

This BMDO/AFOSR sponsored SBIR program was to develop a single-mode wavelength division demultiplexer (WDDM), which would be optimized for the bit-parallel fiber optic network architecture developed at the Jet Propulsion Laboratory (JPL). The bit-parallel wavelength division-multiplexing (BPW) scheme was developed at JPL [1-3] to overcome the limitations of current data communication technologies. This scheme encodes each bit of a byte as a pulse of light with a different wavelength. These pulses are then combined into a single-mode fiber by a conventional WDM technique, along with a shepherd pulse, which travels along with the superimposed pulses and serves to maintain their alignment as they travel along the fiber through nonlinear optical processes. The JPL BPW architecture presents the opportunity for development of a cost-effective wavelength division multiplexing system to be marketed as a standard product for high performance computing network applications. The highlights of the achievements under this SBIR program are:

- A series of single-mode Wavelength Division Multiplexer/Demultiplexer units were designed and prototype modules were fabricated and packaged.
- Established the specifications, and finalized the device structure of the WDDM for bit-parallel computer architecture.
- The bulk ruled reflection high-order Echelle gratings were employed to realize high dispersion, to achieve high diffraction efficiency within a wide spectral range, and low polarization dependent loss (PDL).

- A diffraction limited triplet lens system was designed to serve the functions of simultaneously collimation and focusing, so that, the device cost and size were decreased dramatically.
- A 33-channel fiber array with non-uniform channel spacing was designed to compensate the non-linear effect of angular dispersion.
- Optical Fibers with graded index lens were designed and fabricated to expand the mode field diameter, which increases passband and relaxes the alignment tolerance.
- A thorough thermal analysis and optimization has been performed to achieve athermalized WDM design and packaging.
- In order to further broaden the passband to meet the specification, a 40 channel 100 GHz interleaver-based DWDM were designed and a prototype was built.
- The performance of the interleaver-based demultiplexer was tested.

In brief, this SBIR program was highly successful, and a few modules were completely packaged and tested. Professor Ray T. Chen contacted the JPL team on behalf of Omega Optics. However, it appears that JPL team has closed their program. A set of 32-channel WDM/WDDM modules were successfully used to demonstrate a high throughput bit-serial data transfer between two computers for another program. The detailed final technical report for the project is presented herein.

2.0 INTRODUCTION

Within microprocessors and between chips and boards inside modern computers, data are transmitted in parallel using electronic signals traveling on wires. This becomes unfeasible for long distance links, and therefore, long-distance networks use the conversion of parallel signals to a serial signal, which must be transmitted at a much higher rate than the signals inside the computer. This has placed a bottleneck in communications between computers. Various approaches have been tried, but they usually suffer one of two consequences. If parallel-to-serial conversion is used, higher bandwidth can be obtained by sending packets of data over several links to the destination, and recombine these packets at the destination. However, packets may arrive out-of-order, which increases latency and makes the serial-to-parallel conversion a difficult task. If each bit of a parallel signal is transmitted through a separate parallel wire or optical fiber, the time synchronization between parallel lines becomes difficult or impossible to maintain, due to signal skew.

To address this bottleneck issue, an all-optical bit-parallel WDM (wavelength division multiplexed) single fiber link has been proposed [1-3]. This scheme is unlike the usual WDM format, in which several data streams are imposed onto different wavelengths of light in separate fibers and then combined into one single fiber by an optical wavelength division multiplexer, the WDM. This conventional format suffers the same limitation as an array of parallel optical fibers; because different wavelengths will travel at slightly different velocities even in the same fiber, and the signals will arrive with skew (loss of time synchronization). This prohibits the transmission of a byte as a set of synchronized pulses on different wavelengths, because they will not arrive at the receiver simultaneously and it will be impossible to reconstruct the byte with an acceptable low error rate. A new scheme is needed to avoid this problem.

The bit-parallel (BP) WDM scheme avoids this skew problem by encoding each bit of a byte as a pulse of light with a different wavelength. Then these pulses are combined into a single-mode fiber by a conventional WDM, along with a shepherd pulse, which travels along with the superimposed pulses and serves to maintain their alignment as they travel along the fiber [1-2]. The shepherd pulse is the key concept [2], and is possible because of developments in nonlinear optics and the availability of powerful laser diodes. The technical specifications for

the various components and devices have been determined, and discussed in detail by the JPL group [3]. This SBIR project was to address the technical problems in the design and manufacture of the WDM components needed to decode and convert the bit-parallel optical pulses into electrical pulses at the receiving end of the optical fiber link.

2.1 BASIC ELEMENTS OF THE BIT-PARALLEL WDDM.

For the JPL bit-parallel architecture, the 8 bits of a byte will be launched into a single optical fiber without parallel-to-serial conversion. These parallel pulses will be launched simultaneously on separate wavelengths. More than 8 channels are needed due to error correction schemes and/or the need for spare channels in case of failures in the transmitter or receiver. (10 wavelengths are needed in order to be compatible with the Myrinet architecture, and 12 for HIPPI-6400.) Anticipating the use of erbium-doped fiber amplifiers in the long-distance links, the entire set of channels must lie in the band from 1535 nm to 1560 nm. Separation between these channels must thus be 2 nm or less, and for compatibility with international standards, will be chosen on the ITU channel grid [3].

In order to maintain the time alignment of the parallel pulses, a strong pulse at wavelength 1542 nm will be launched into the fiber simultaneously with the bit-parallel pulses. Corning DS single-mode optical fiber has been chosen for the demonstration project, and since it has a dispersion coefficient of around 2 ps^2/km, the pulses would tend to travel at different velocities and spread out (or separate) from each other. However, the strong pulse will interact with these weaker pulses by a nonlinear effect, and will have the effect of keeping them all aligned with each other, traveling along the fiber together. This effect motivates the designation of the strongest pulse as the shepherd pulse.

At the receiving end, the shepherd pulse must be discarded, then the parallel pulses separated into different directions according to wavelength (by the wavelength division demultiplexer (WDDM)), and then detected with fast photodetectors for conversion into electrical pulses. This architecture imposes requirements on the WDDM device, which challenge the capabilities of previously-demonstrated devices in two respects. The first is the

need for single-mode as opposed to multimode operation, and the second is efficient output coupling to an optical fiber array or to a photodetector array.

Wavelength division multiplexing (WDM) and demultiplexing (WDDM) devices are considered to be two of the key elements for enhancing the transmission bandwidth of optical communications and sensor systems. During the past 20 years, various types of WDMs and WDDMs have been proposed and demonstrated [4-21]. Recently the technique for producing spatially multiplexed phase gratings based on polymer-based waveguide holograms for WD(D)M applications has been reported. Unlike electrical interconnects, WDM-based optical interconnect systems do not have an industrial standard to set the operation protocol governing the wavelength separation. Different companies are using different wavelength separations that fit into the WDM technologies employed. For example, AT&T released a WDM module with a wavelength separation of 0.6 nm centered at 1.55μm. Other WDMs such as the ones produced by 3M, POC and IBM have a wavelength separation as large as 30 nm. Such a trend will continue until a unifying technology appears. To achieve the set wavelength separations, different companies employ different working principles. Furthermore, due to the involvement of a myriad of different technologies in WDM design, the optoelectronic packaging issues become complicated, costly, and even vulnerable in some cases. This is primarily due to the involvement of free space optical interconnects in packaging design.

In this Phase II research program, 32 and 40 channels single-mode wavelength division demultiplexers (WDDM) have been developed, which would be optimized for the bit-parallel fiber optic network architecture. The high channel counts make possible to support multiple 8-bit parallel data simultaneously. There is an opportunity of commercialization of these WDDMs in the growing market of Dense-WDM fiber-optic communications.

3.0 TECHNICAL OBJECTIVES

In order to satisfy the needs of this particular BPW architecture, strict component requirements must be met, which motivates the continued development of single-mode WDDM technology.

- Development of an input collimator/output-focusing lens, which could accept an input signal from a single-mode optical fiber and couple the output signals into corresponding output fibers simultaneously.
- The proper design of a bulk diffraction grating with the maximum diffraction efficiency and minimized polarization dependent loss. The bandwidth of this grating should cover the whole C band (1528 to 1560 nm).
- The design and fabrication of an output single-mode fiber optic array to compensate the non-linear effect of angular dispersion.
- Thermal analysis and optimization to realize athermalized WDDM devices.
- Design graded index lensed fibers to broaden the optical passband of single-mode WDDM, which is very important for maximizing spectral efficiency and relaxing the tolerance on wavelength control.
- Design and fabricate product packaging. This is the most challenging objective. Successful athermalized packaging design offers the potential to make a cost-effective product for data and telecommunications in defense and commercial markets
- Device characterization and performance measurement
- Improve optical design and achieve passband broadened DWDM

Only by developing these new features of WDDMs can the specific requirements of the JPL bit-parallel ShuffleNet architecture be met.

4.0 THE WDDM SPECIFICATIONS

Number of channels	32 or 40
Fiber connections	Single-mode, Corning type SMF-28
Channel center frequencies	191.2 THz to 194.3 THz: in 0.1 THz steps. (1542.52 to 1567.53 nm)
Channel spacing	100 GHz
Bandpass for 196.1 THz channel	3 dB points: 25 GHz typical 1 dB points: 13.75 GHz typical
Adjacent-channel isolation	40dB min., 45 dB typical, anywhere within bandpass.
Data transmission bit rate	at least 10 G bit/sec (3 dB point), any channel
Insertion loss	6 dB max, 4.5 dB typical, all channels at center wavelengths
Polarization-dependent loss	< 1.25 dB, all channels at center wavelengths
Return loss	-40 dB max.
Operating temperature range	-5 to +60° C
Storage temperature range	-40 to +85°C
Dimensions	266.7x76.2x22.9 mm (10.5×3.0×0.9 inch)
Frequency accuracy	±6.3 GHz (Each channel over entire operating temperature range)

5.0 COMPETING APPROACHES TO (MUXS)/(DEMUXS)

There are several competing technologies for making MUXs/DEMUXs under active developed [4]. These technologies include multiplayer dielectric thin-film filters, Bragg grating filters [5-10], phased-array-waveguide-gratings [11-17], and diffraction gratings [18-21]. The important characteristics of WDMs used in telecommunications systems are insertion loss, polarization dependent loss (PDL), temperature effect, passband flatness, crosstalk, packaging size, and cost. Brief physical bases of these different technologies are provided.

5.1 Interference filters

Thin-film dielectric devices are the most broadly deployed filters for low-channel-count DWDM systems in the 400- and 200-GHz channel spacing regime. As Figure 5.1 shows, two or more resonant cavities are separated by reflective dielectric thin-film layers, which have quarter-wave thickness, and alternating high and low indices.

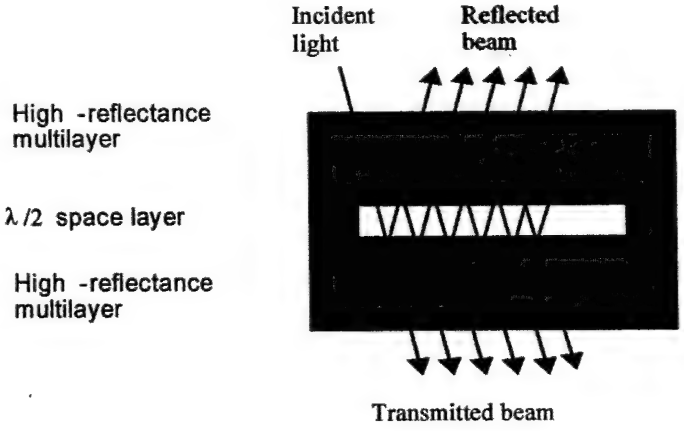

Fig. 5.1 Interference filter.

These resonant cavities form a bandpass filter, transmitting a specific wavelength and reflecting all other wavelengths. This mature technology offers good temperature stability (<0.002 nm/°C), channel-to-channel isolation, and a flat passband. It's primary challenge is to decrease the channel spacing to 100 GHz and below, with good yield, as well as increasing the channel count beyond 16.

5.2 Arrayed waveguide gratings (AWGs)

The principle of array waveguide gratings (AWGs) is interferometry. Figure 5.2 shows the structure of an array waveguide WDM [22]. The wavelength-dependent phase delays are caused by the length differences of the arrayed waveguides. The varied wavelengths with different phase interfere with each other in such a manner that each wavelength achieves maximum energy at a designed position. The separated wavelengths can be coupled into a fiber array. Since AWGs are fabricated using stander IC technologies, these devices lend themselves to high integration and consequently large channel counts. Channel spacings are typically 100 GHz, although 50 GHz devices are also available. But temperature stability is often a concern, requiring active temperature controller.

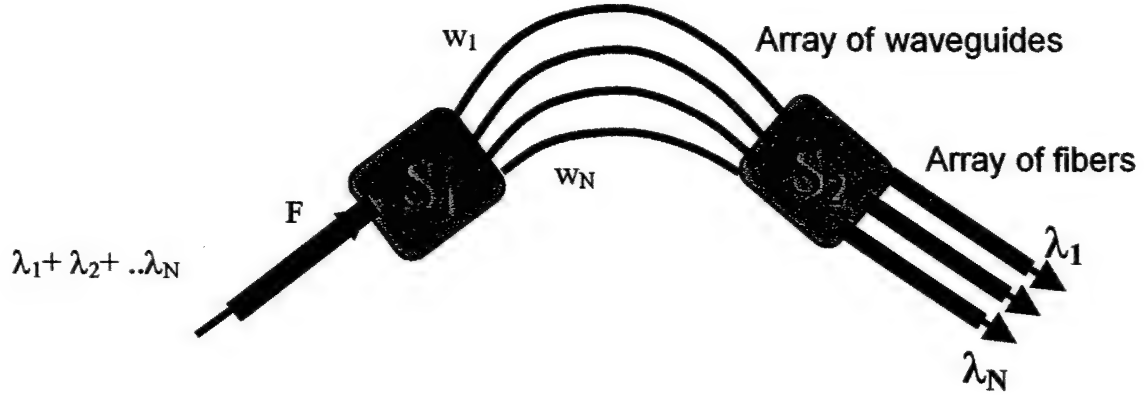

Fig. 5.2 Array waveguide grating

5.3 Fiber Bragg gratings (FBGs)

The dispersion in fiber Bragg grating is achieved by periodically varying the index of refraction of a fiber segment. Figure 5.3 shows how the fiber gratings are made. The periodic variation of index is formed by exposing the Germano-silicate core of the fiber to an intense periodic ultra-violet (UV) pattern. Insertion loss and uniformity of fiber Bragg grating based devices are very good because they are fabricated from standard single-mode fiber. The long-term stability is an issue due to the stability of tuning.

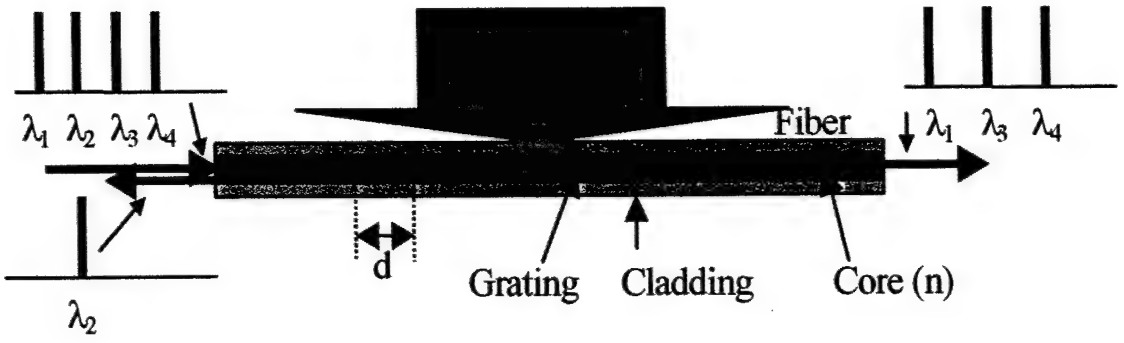

Fig. 5.3 A fiber is exposed under UV light to create index modulation [22].

5.4 Diffraction-gratings

Diffraction-grating devices feature a finely ruled grating that diffracts the incident beam into different angles and positions. As shown in Figure 5.4, each wavelength channel corresponds to a unique diffraction angle, and that can be collected by individual fibers. Our approach focuses on diffraction grating-based DWDM. This technology has several major advantages, including low and uniform insertion loss across the entire passband, superior crosstalk, accurate wavelength, athermal performance and scalability. The low channel count devices can be upgraded to high-count devices simply by installing more fibers. Table 5.1 gives a comprehensive comparison among technologies for making MUXs/DEMUXs [23].

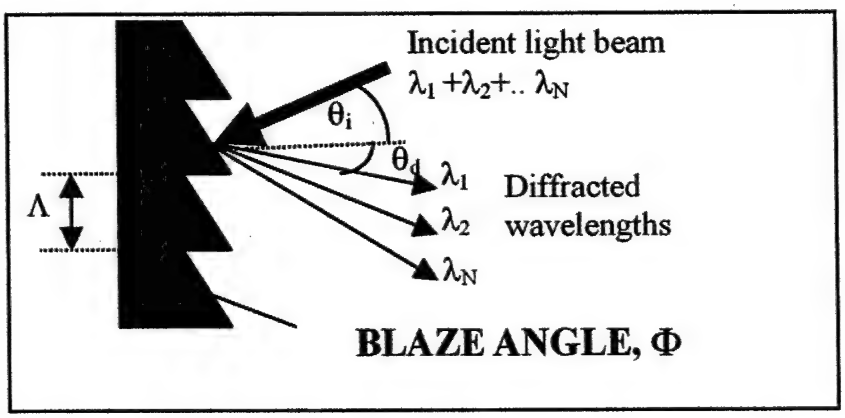

Fig. 5.4 Diffraction grating based WDM; different wavelength is diffracted into different angles and positions

TABLE 5.1 COMPARISON AMONG VARIOUS TECHNOLOGIES FOR MAKING DWDMS [23]

Technologies	Advantages	Disadvantages
Thin-film dielectric interference	Mature technology Good temperature stability Good wavelength selectivity Very good PDL Flat passband	Difficult to product narrow channel spaced filters (<100GHz) Insertion loss is not uniform for high channel counts Filters can only be manufactured for a fixed wavelength Not scalable
Planar array Waveguide	Uses IC fabrication processes. Scalable to high channel counts Can integrate multiple functions on a single chip	Difficult fiber interface Capital-intensive Requires large infrastructure Need temperature controller
Fiber Bragg Gratings	Mature technology	Mechanical stability problem High back reflection; must use isolator.
Fused, cascaded Mach-Zehnder Interferometers	Low insertion loss and polarization effects Can produce very narrow channel spaced devices Easy coupling to fiber Generates filter "comb" rather than wavelength-specific filter	High channel count devices require cascaded devices resulting in a larger form factor device.
Diffraction Gratings	Low & uniform insertion Loss Best crosstalk, less than –40dB Good temperature stability Scalable	Devices can be bulky Typically used in a free space mode requiring careful assembly techniques.

6.0 DIFFRACTION GRATING BASED WDDM CONFIGURATION

6.1 WORKING PRINCIPLES

In regard to the structure of grating-based MUXs/DEMUXs there are two main types: the Czerny-Turner structure, which has different lenses for input and output, and the Littrow structure, which has one common lens. The structure for the Czerny-Turner type WDM is shown in Figure 6.1. Light signals with different wavelengths from different channels are launched into a fiber array. The light signals from the fiber array are collimated in different directions by a lens and the grating diffracts these beams in a given direction. Another lens focuses the light beams into a single fiber. This operates as a multiplexer. When the directions are reversed, the device functions as a demultiplexer, in which light signals with different wavelengths traveling in a single fiber are collimated by a lens and guided in different directions by a grating. Another lens launches these beams into separate fibers.

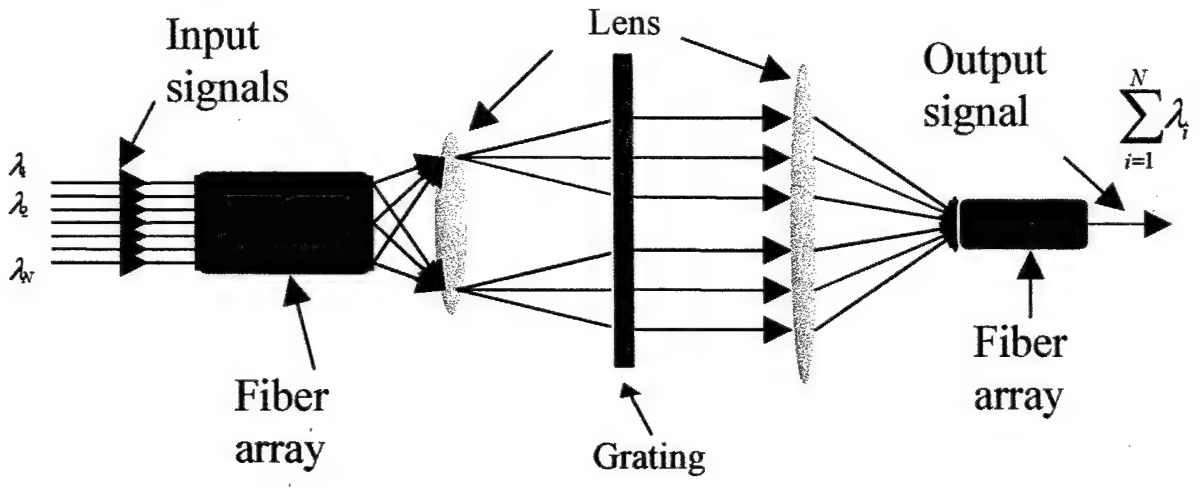

Fig. 6.1 The diagram for the structure of the Czerny Turner typeWDM.

To examine the operating principle of the Littrow structured grating-based WDM multiplexers/demultiplexers, we refer to the structure shown in Figure 6.2. An input fiber and multiple output fibers are arranged on the focal plane of the lens. Wavelength-multiplexed light signals from the input fiber are collimated by the lens, and reach the diffraction grating. The

light is angularly dispersed, according to different wavelengths, and simultaneously reflected. Then the different wavelengths pass through the lens and are focused to their corresponding output fibers. Each wavelength is fed to one individual output fiber. This functions as a demultiplexer. When working in the reverse direction, the device serves as a multiplexer. Since Littrow WDM multiplexers/demultiplexers use fewer components, they are more cost-effective.

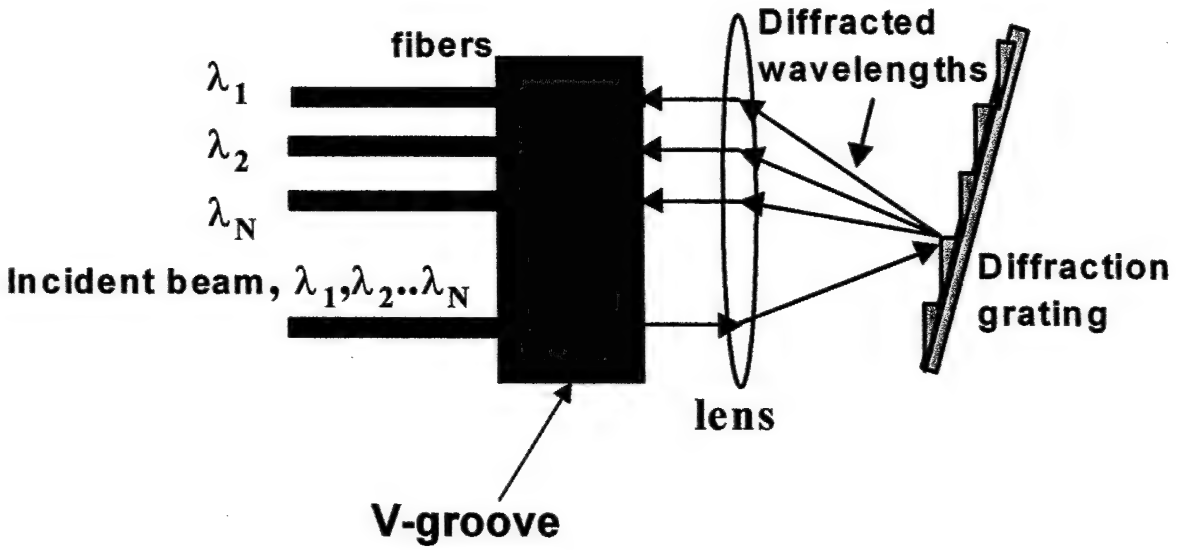

Fig. 6.2. The diagram for the structure of the Littrow type WDM.

6.2 KEY PARAMETERS

Some of the key parameters are independent of the multiplexing/demultiplexing structure. An optimal design must take into account the following constraints: (a) nominal wavelengths or frequencies of each channel; (b) number of channels; (c) channel separation, in wavelengths or frequency; (d) passing bandwidth of each channel, or channel capacity; (e) insertion loss; (f) the transmission spectrum over the passing bandwidth of each channel; (g) isolation among channels, or the power level due to crosstalk; (h) polarization-dependent loss (PDL); (i) for passive devices, sensitivities due to ambient temperature, pressure, humidity variation, etc.; (j) return loss (RL); (k) the power damage threshold, or the maximum optical power for each channel; and (l) pulse-broadening of the device. Such other issues as physical geometry, weight, input/output interfaces, and greater or lesser cost depending on applications also directly affect the choice of design spaces.

WDM systems for telecommunication tend to use a 100*GHz* frequency grid centered at 193.1*THz* optical frequency, aiming at a 10*Gbs* capacity per channel, as recommended by ITU-T. This constrains the choice of (a)-(c) even though devices with channel spacing less than 50*GHz* have been developed. Much wider channel spacing for shorter-distance data communication may be a good compromise for operational and economic reasons. For grating-based WDM multiplexers/demultiplexers these parameters are mostly determined by the dispersion ability of the grating, subject to the constraints of the physical size of the device. The loss spectrum of a passive device is generally sufficient to characterize the requirements (d)-(h) above, when appropriate out-coupling interfaces are taken into consideration. In the remaining part of this section we discuss these terms in detail with experimental data obtained in our efforts to optimize the design for grating based WDM multiplexers/demultiplexers. Material selection and engineering are also important elements by means of which the performance of the device is optimized. In practice, packaging issues should be considered along with the other criteria.

Such other issues as return loss, pulse broadening or bit rate, power damage threshold, physical size and weight, and cost affect the design of devices. As a rule of thumb in fiber optics, a polished end angle of 8 degrees will reduce the return loss to better than 40 dB for a single-mode devices. Since the grating-based WDM multiplexer/demultiplexer works on the principle of grating dispersion, when a light pulse passes through the device, the pulse will be broadened. The pulse broadening can be reduced by contracting the device. The physical size and weight can be reduced by increasing the angular dispersion ability of the device. A good WDM multiplexer/demultiplexer must optimize all the key parameters discussed above.

6.3 DEVICE CONFIGURATION

A simplified diagram of the optics of the DEMUX is shown in Figure 6.3. Thirty-two-channel WDM wavelengths were introduced into the DWDM device by a single-mode fiber with an FC connector, and then were collimated by an optimized diffraction limited triplet lens. The same lens functions as the focusing lens for the demultiplexed signals. We used a 22^{nd}-order echelle grating to demultiplex 32 optical signals within the C band with 100-GHz channel spacing. The working wavelength range was from 1542.94 to 1567.95 nm at the vacuum. The ITU fiber-optic telecommunications channel standard [24, 25] determined the wavelength

choice. In order to eliminate multiple alignments for individual fibers and to increase throughput, we deployed a 33-channel silicon V-grooved fiber array, which was designed to have variable fiber spacing because of the nonlinear effect of the angular dispersion [26]. The one-layer fiber array has one input single-mode fiber at one end to introduce the multiplexed signals, and 32-single-mode output fibers to receive the 32 demultiplexed signals. The spacing of the fiber array was designed to be non-uniform varying from 140.1 to 164.4 μm to obtain accurate center wavelength within the ITU grid.

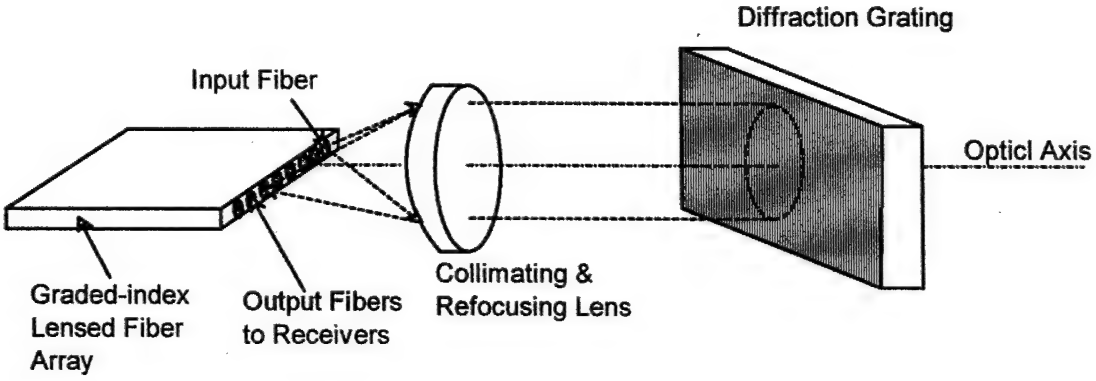

Fig. 6.3 The simplified schematic drawings of a 32-channel single-mode-in and single-mode-out DWDM.

6.3.1 High-order echelle grating design principle and parameters

A high-order echelle grating has several special properties, which make it an excellent diffraction component for WDM diffraction. Most apparent is its high dispersion, which permits compact optical systems with a high throughput and high resolution. In addition, because it is never used far from the blaze direction, the grating efficiency remains relatively high over a large spectral range. Furthermore, when the grating is operated at higher orders, it is nearly free of the polarization effect. Under the Littow mount condition, when the incident angle is the same as the diffraction angle, another useful property comes into play: one lens can both collimate and focus simultaneously, resulting in lower cost and decreased packaging size for the WDM system.

Usually, the higher the grating order, the smaller the polarization effect of the grating. But any given grating order is also limited by certain factors such as its working spectral range. We calculated the corresponding grating working order to cover the C band spectral range (from 1528 nm to 1560 nm). When the extremes of the C band are represented by λ_1=1528 nm and

λ_2=1560 nm, the formula for calculating the grating order for a certain spectrum range can be expressed as

$$m = \frac{\lambda_1}{\lambda_2 - \lambda_1} \tag{6.1}$$

So that the spectrum of the C band signal λ_2 operating at order m does not overlap with the spectrum of signal $\lambda_1$when operating at m+1 order, m must be less than 47. On the other hand, we must leave room to fully reduce the noise caused by the scattering of adjacent orders.

We chose 22 as the grating working order, and the grating groove spacing (18μm) is large compared to the operating wavelength (1.5μm). This in turn implies that scalar theory of diffraction may be used. A groove facet is a small mirror or a small prism, but behaves in the same way as a large one. When the widths of the grooves are comparable with the wavelength of light this assumption is no longer valid, because the oscillations of the electrons are impeded or curtailed by the boundary of the facet. In practice when the groove spacing is less than about three times the wavelength, the efficiency curves for the two polarizations differ dramatically, and the "blaze wavelengths" differ. Figure 6.4 shows our measurements of the grating efficiency across all working wavelengths. The grating efficiency varies from 45%-80% within the whole

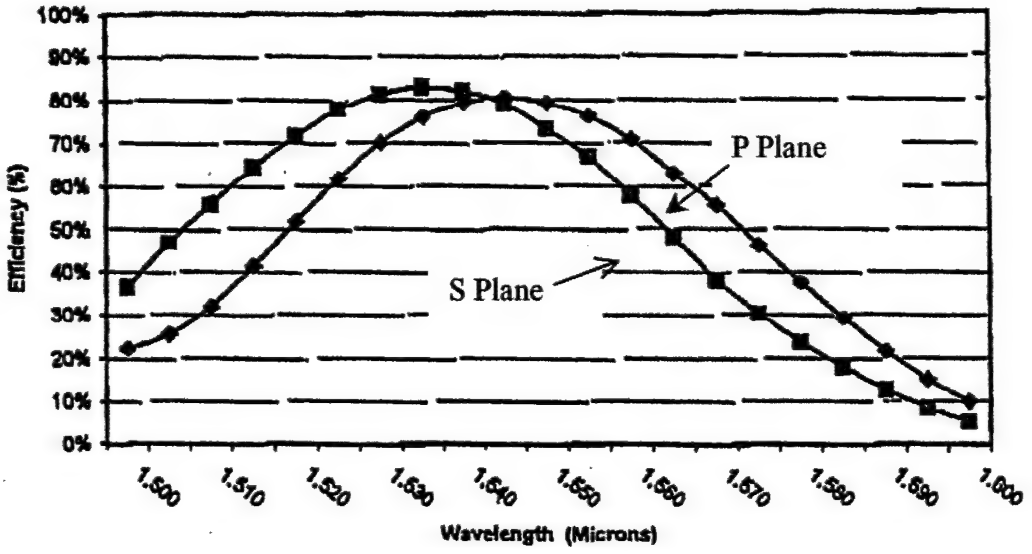

Fig. 6.4 Diffraction efficiency of the 22nd echelle grating

working wavelength range (1542.95-1567.95 nm). By using 22nd-order grating, the diffraction efficiency is almost independent of the polarization of incident light. The reflection grating diffraction equation is [27]

$$n\Lambda(\sin\theta_i - \sin\theta_d) = m\lambda, \tag{6.2}$$

where in, incident angle is θ_i, diffraction angle is θ_d, facet angle is ϕ, where all three are measured from the grating normal; m is the order of diffraction, λ the wavelength, Λ is the groove spacing, and n is the refraction index of the medium containing the incident and diffracted rays. Here, n=1. We found the angular dispersion by taking the first-order derivative of θ_d

$$\frac{d\theta_d}{d\lambda} = -\frac{\sin\theta_i - \sin\theta_d}{\lambda\cos\theta_d}. \tag{6.3}$$

For the Littrow condition $\theta_i = -\theta_d$, and angular dispersion is

$$\frac{d\theta_d}{d\lambda} = \frac{2\tan\theta_d}{\lambda}. \tag{6.4}$$

The larger the diffraction angle, the greater the angular dispersion. In our design of the 32-channel DEMUX, the incident and diffraction angles are $\theta_i = -\theta_d = 62.4°$ at the center wavelength of 1555.75 nm, which is the *16th* channel of our device. The angular dispersion of the grating at the central wavelength was 0.152°/nm.

Blazed grating redirects the incident light in the direction of a chosen diffracted order if each groove is formed appropriately. Thus in a reflection grating each groove consists of a small mirror inclined at an appropriate angle. The blaze condition is satisfied when the angle of incidence with respect to the facet normal is equal to the angle of reflection from the facet (See Fig. 6.5); *i.e.*

$$\theta_i - \phi = \theta_d + \phi; \tag{6.5}$$

$$\phi = \frac{\theta_i - \theta_d}{2} \quad \text{or} \quad \theta_d = \theta_i - 2\phi \tag{6.6}$$

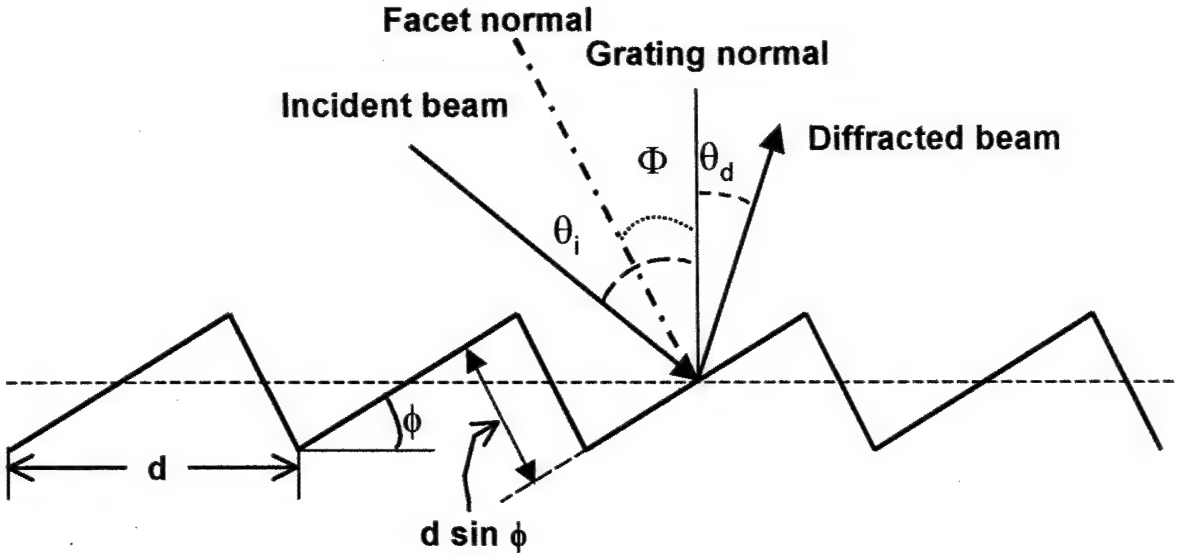

Fig. 6.5 Configuration of a blazed grating

Considering the Littrow mount, $\theta_i = -\theta_d$, so $\phi = \theta_d$, which is the situation depicted in Figure 6.6. The grating blaze angle was 64°.

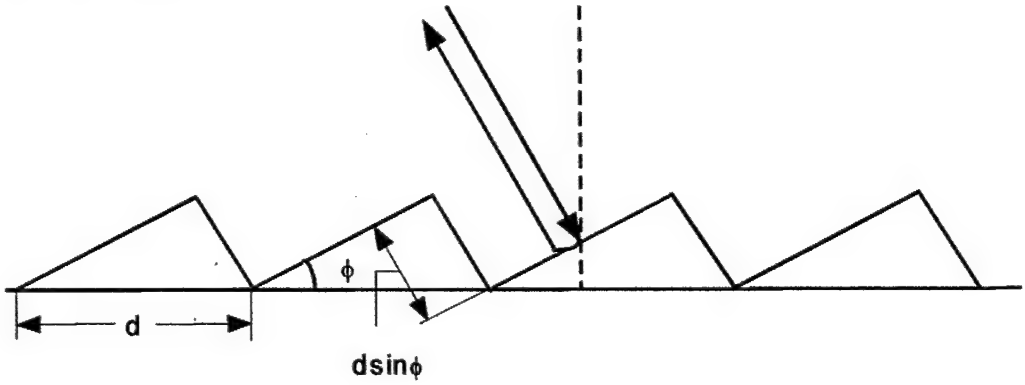

Fig. 6.6 A blazed grating used in the Littow mounting

6.2 Optical design

Figure 6.7 shows a cross section of the optics of the demultiplexer. The vertical line at the left of this figure is the focal plane, and the front end of the fiber array (not shown) is in this plane. Light leaves the input fiber and is collimated by the lens. The grating disperses the light angularly into its constituent frequencies; the rays of one signal are shown in the diagram. The

light for this frequency, 194.3THz, is focused by the lens onto an output fiber. For simplicity, rays for the other 31 channels are not shown.

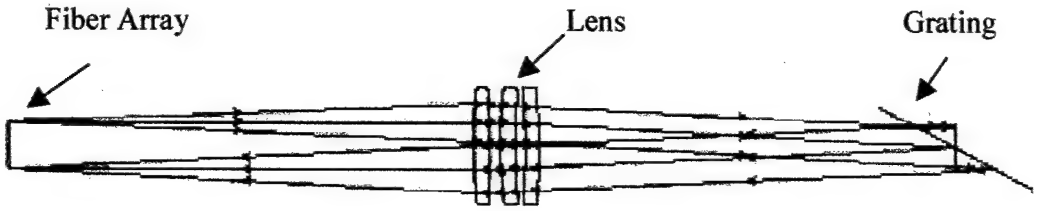

Fig. 6.7 The optical layout of the demultiplexer. All the optical designs for lens, fiber array, and grating are good for demultiplexing 32 wavelength within C band.

Because the size of the device is essentially proportional to the spacing of the fibers, which is only 140.1 μm, the fiber spacing could have been reduced to less than this value, with a consequent reduction in size and weight of the device.

The lens is telecentric, i.e. the input beam and all output beams are nearly parallel to the optical axis. This fact has important consequences. First, insertion loss is minimized because all of the output beams are perpendicular to their respective fibers. Second, the frequency of a channel is invariant with respect to changes in focus. Since there are small changes in focus with changes in temperature, the frequency will not be a function of temperature.

The linearity of the angular dispersion among different wavelengths is critical for achieving uniform channel spacing, and then uniform passband. Equation (6.3) shows that angular dispersion is not a linear function of diffraction angle. The condition for achieving linear angular dispersions among different channels can be found by taking the second-order derivative of the diffraction angle, *i.e.*

$$\frac{d^2\theta_d}{d\lambda^2} = \frac{\sin\theta_i . \sin\theta_d (\cos\theta_i - \sin\theta_d)}{\lambda^3 \cos^3\theta_d}. \qquad (6.7)$$

When the diffraction angle in the air is zero, the best angular dispersion linearity can be achieved. In our design $\theta_d = 62.4°C$, so the spacing was non-linear and varied from 140.1 to 164.4 μm. Figure 6.8 shows the spacing between each individual channels

The focal length f of the lens can be calculated by Equation (6.8) once the fiber spacing Δy and wavelength increment $\Delta\lambda$ between adjacent channels is known.

$$f = \frac{\Delta y}{\Delta \lambda} \frac{\lambda}{2 \tan \theta_d} \qquad (6.8)$$

The above formula shows that the focal length of the lens is directly proportional to the fiber spacing and to the tangent of the angle of diffraction. Thus, in order to make the lens small, one can use closely spaced fibers and a large diffraction angle. For blazed grating, the diffraction angle is approximately equal to the blaze angle ϕ. For the center wavelength λ=1555.75 μm, $\Delta\lambda$=0.8 nm, Δy=151.6μm, we can obtain f=72.5 mm.

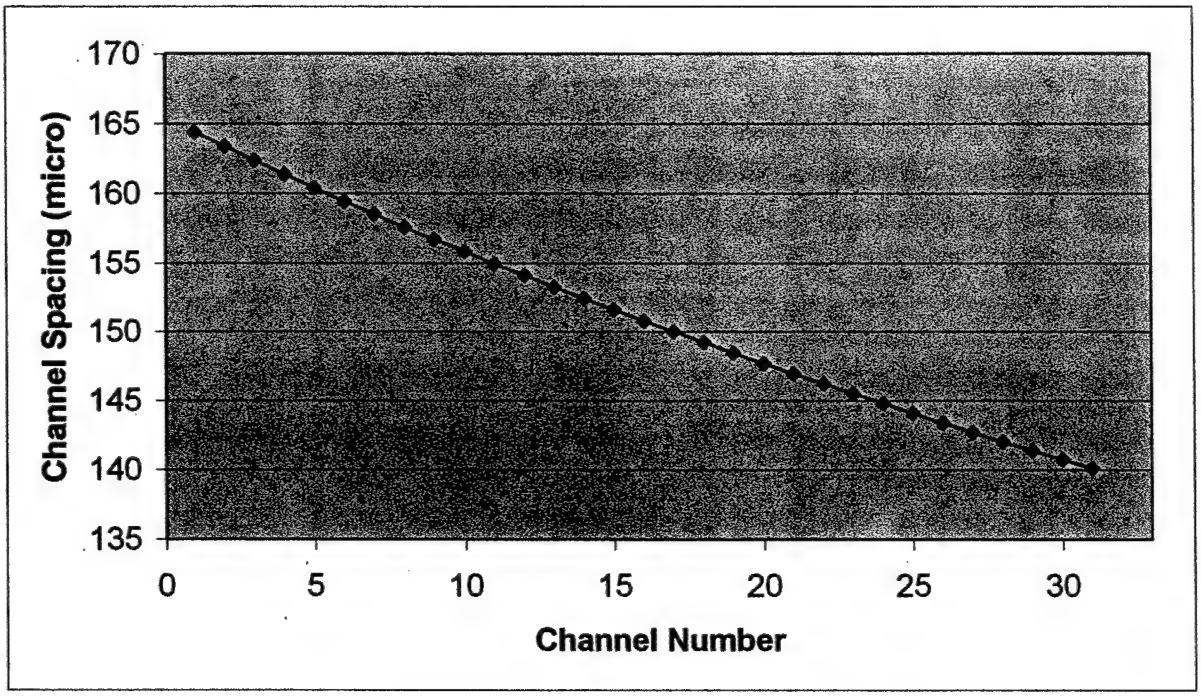

Fig. 6.8 Non-uniform channel spacing of fiber array

The spot diagram for channel 1, 2, 16, 31, 32 is shown in Figure 6.9. The spots across the whole wavelength range are diffraction limited. The average light spot diameter is 10μm, much smaller than the core size of graded-index lensed fiber (45μm). This factor eased the lateral and

longitudinal alignment greatly. Since the mode field diameter of this special fiber was increased, the numerical aperture is decreased to 0.032 restricting the tolerance of the angular alignment.

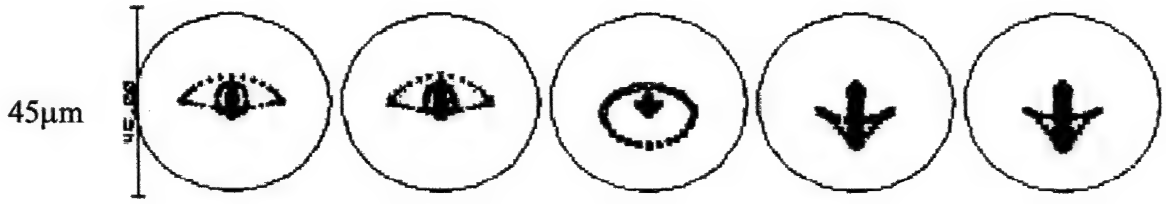

1542.522 1543.319 1555.329 1566.712 1567.531

Fig. 6.9 The spot diagram for the diffracted wavelengths at two ends and the middle of the spectral range. The circles outside of individual spots represents the core size of graded indexed lens fiber.

7.0 GRADED INDEX LENSED FIBER DESIGN FOR PASSBAND BROADENING

7.1 Passband broadening

Broadening and flattening of the passband in WDM is key to maximizing spectral efficiency and relaxing the tolerance on wavelength control in the networks [27]. Typical grating-based WDMs have passbands or spectral responses that are generally highly peaked with a slow roll-off in their wavelength response. This effect results from the diffraction response of the associated grating element that separates the wavelengths, from the transmission response of intervening optical lens elements, and from the receiving optics. Such responses do not use the full bandwidth of the most multiplexers and demultiplexers. As a result, it is often difficult to specify wavelength tolerances for associated components such as laser light sources, amplifiers and other optical components.

The width of the optical passband is mainly determined by the filling ratio "*F*", *i.e.,* the ratio of the receiving fiber core diameter to the distance between the centers of two neighboring fibers. The larger this ratio, the larger the passband. In order to increase passband, one can either increase the core diameter or decrease the central spacing between adjacent output fibers. The output image reshaping and broadening approach [29,30] has been used for array waveguide-based WDM. For diffraction grating based WDM, in order to increase core diameter or increase mode field diameter (MFD), one can use thermally expanded core fibers [31, 32], use graded-index lensed fibers [33-36], or defocus the focused beam spots at the focal plane [37]. In order to decrease the fiber spacing, we can strip the coating or etch the cladding to the smallest allowable size. But one can neither increase the core diameter nor decrease the channel spacing without limitation. There is an intrinsic trade-off between passband and crosstalk. A lower crosstalk requires a wider separation between the output fibers and, therefore, necessarily higher linear dispersion, resulting in proportionally narrow bandwidth.

The Littrow mount geometry of the WDM design provided aberration-free image systems. The light spots of diffracted beams are almost identical in size to the cores of the fibers. In this case, the optimized value of this ratio F=0.667.

Figure 7.1 shows the geometrical layout of the fiber array. D is the fiber cladding diameter, d is the fiber core diameter; and b is the distance between the centers of two adjacent fibers. For the most compact fiber array layout, $b=D$. For typical single-mode fibers, the value of

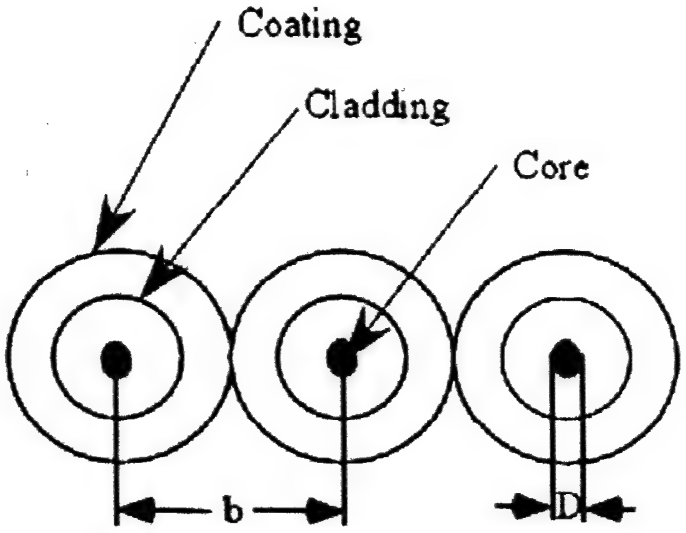

Fig. 7.1 Geometrical layout of fibers in compact fiber array.

d is approximately 9.5 μm; cladding diameter D is 125 μm, which means b is usually not smaller than 125 μm. The resulting filling ratio is:

$$F = \frac{9.5}{125} = 7.6\% \tag{7.1}$$

For a 100-GHz (0.8nm) single-mode DWDM, the corresponding 3dB passband is only 0.06nm. Generally, one needs a 0.2nm 3-dB passband to compensate the wavelength shifts in laser sources. Therefore, it is of the utmost importance to find solutions for broadening the passband of grating-based single-mode DWDM.

7.2 Design of Graded-index lensed fibers (GILFs)

Cascading a graded-index fiber (GIF) to a single-mode fiber to either expand or reduce the mode field diameter (MFD) of the single mode fiber has been reported for fiber/waveguide [34] and laser/fiber coupling [35]. For WDM application, one can use GIFs as spot expander to increase the 1dB optical passband.

Figure 7.2 shows the beam propagation through lens media [38]. The input plane contains the end face of a single-mode fiber and the beam waist $w_{in;}$ the output plane contains the final beam waist w_{out} which is formed after passing through a square-law lens medium. The square-low dependence of the refractive index of the lens media can be expressed as:

$$n(r) = n(1 - g^2 r^2)^{\frac{1}{2}}, \tag{7.2}$$

where, n is the refractive index on the lens axis, and r is the radial position from the axis.

The focusing parameter g can be expressed as

$$g = \frac{\sqrt{2\Delta}}{r}, \tag{7.3}$$

where in, Δ is the relative refractive index difference between the core axis and its perimeter at r.

When the fiber-lens is fused to a single mode fiber directly, the final waist size and its location can be expressed as [39]:

$$w_{out} = \frac{\lambda}{ng\pi w_{in}(\sin^2(gd) + (\frac{\lambda}{\pi w_0^{\,2} ng})^2 \cos^2(gd))^{\frac{1}{2}}}, \tag{7.4}$$

and

$$z_w = \frac{n_2(1 - (\frac{\lambda}{\pi w_0^{\,2} ng})^2)\sin(gd)\cos(gd)}{ng(\sin^2(gd) + (\frac{\lambda}{\pi w_0^{\,2} ng})^2 \cos^2(gd))}. \tag{13}$$

A quarter-pitch length of graded-index fiber acts as a collimator that can expand mode field diameters (MFDs) of single-mode fibers (SMFs). Figure 7.3 shows the direct cascading of a single mode fiber and a graded-index multimode fiber.

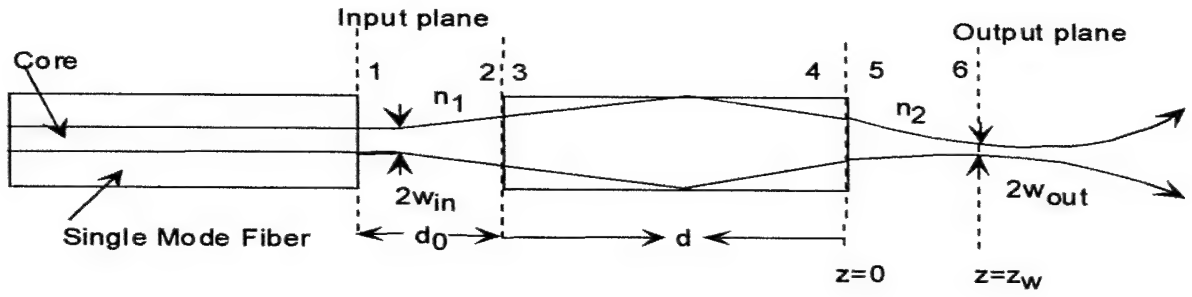

Fig. 7.2 Beam propagation through lens media following Kogelnik's ABCD law.

The period (1 pitch) of a ray trajectory is given by $2\pi/g$. Substituting the length of a quarter pitch $d=\pi/2g$ in Equations (7.4) and (7.5), yields $z_w=0$, and Equation (7.6) can be derived:

$$w_{in}w_{out} = \frac{\lambda}{\pi n g}. \tag{7.6}$$

This relationship indicates that the product of the input and output mode-field diameters is inversely proportional to focusing parameter g. If the input MFD is smaller than the fundamental MFD of the graded-index fiber (GIF) it will expand; if larger, it will contract. So g is a significant parameter. From Equation (7.5), one can find out that smaller the value of difference

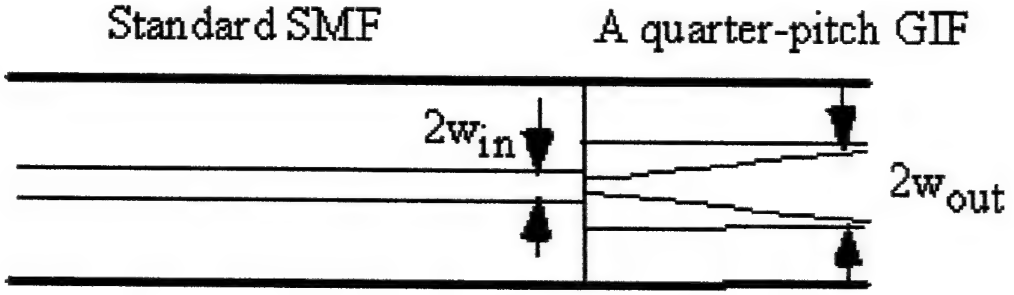

Fig. 7.3 Cascading a SMF with a quarter-pitch length of GIF.

in refractive index Δ, the smaller will be g. Figure 7.4 shows the respective different output MFDs when varying the value of g and the MFDs of a input fiber. If a standard single mode fiber (MFD=10.2 μm) is cascaded with a Corning multimode fiber having core diameter of

50μm (g=0.053), the output MFD of GILF has a value of 24.3μm; if a standard single mode fiber is cascaded with a Corning multimode fiber having core diameter of 62.5μm (g=0.0057), the

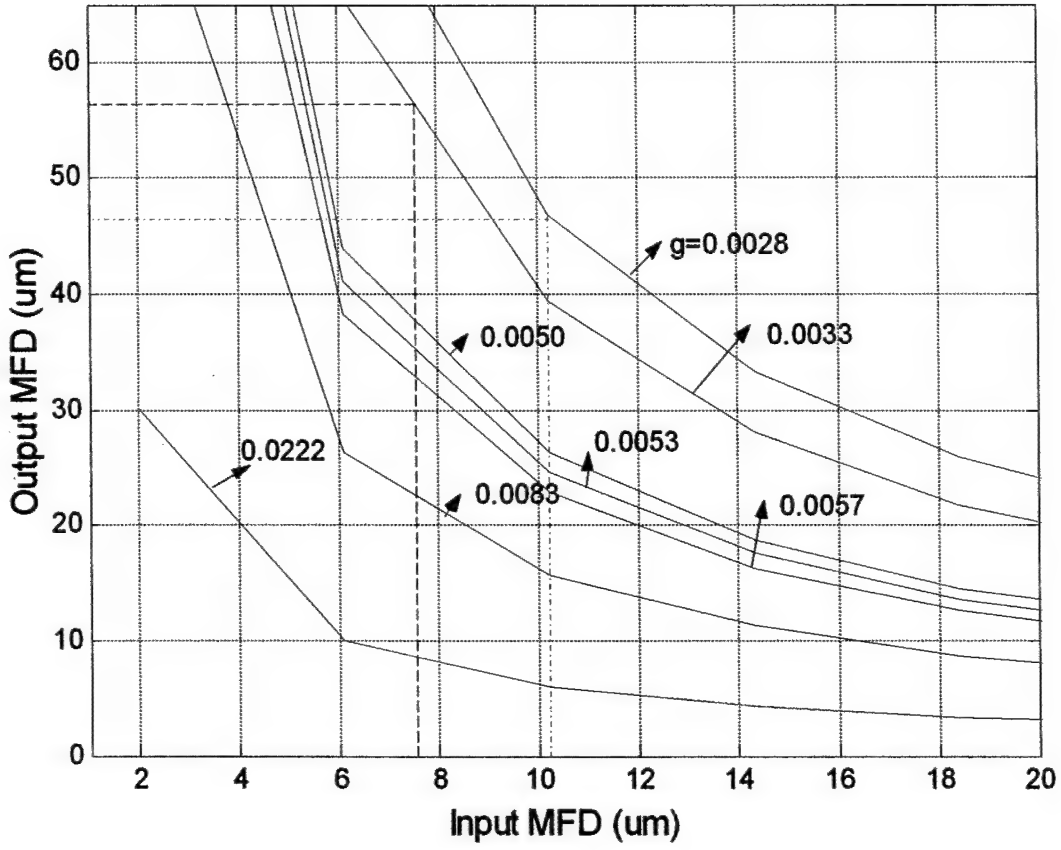

Fig. 7.4 Output MFD of a graded-index lensed fiber with different values of g. When g=0.0033, for dispersion shifted fibers (MFD = 7.6 μm at 1555nm), the output MFD is 57 μm; for the standard single mode fiber (MFD =10.2μm), the output MFD is ~ 47μm.

output MFD of the GILF is 22.9μm. This figure clearly shows that, for a given the input MFDs, the smaller the value of g, (*i.e,* the smaller the value of Δ), the larger the output MFDs can be obtained.

The different output MFDs was also calculated by varying the MFDs of input fibers while keeping the value for g fixed. For instance, if dispersion-shifted fibers (DSFs), which have a smaller MFD (7.6μm), are cascaded to specially made graded-indexed fibers (GIFs) (g=0.0033), larger output MFDs (57μm) are obtained. On the other hand, if standard single-

mode fibers are cascaded to the same GIFs, the output-MFDs are only 40μm. When one decreases the value of g to 0.028, the output MFDs can reach 47μm. Therefore, the conclusion is that DSF or GIF with a smaller value of g are always preferable to expand the output MFDs in GILF design. The GILFs in WDM design have MFDs of 47 μm. The filling ratio was increased from 8.2% to 38%.

8.0 THERMAL STABILITY ANALYSIS AND COMPENSATION

When temperature changes, the insertion loss and center wavelength may change accordingly. The center wavelength shift is caused mainly by the change of groove spacing of the grating. The change of insertion loss is due to the thermal variation in lens focal length, and the image shift in vertical direction caused by the difference of coefficient of thermal expansion (CTE) of lens and its supporting material. It is shown in this section that it is possible to eliminate or reduce the thermal effect by careful optical design, and selection of the materials for making the grating, lens, and housing.

8.1 Central wavelength shift of individual channels

The thermal expansion of the grating can be calculated by equation (8.1)

$$\Lambda = \Lambda_0(1+\beta\cdot\Delta T) \qquad (8.1)$$

Where β is the CTE of grating, ΔT is the temperature change. Assuming the incident and diffraction angle remain constant with temperature, and combining the temperature derivative of Eq. (6.2) and Eq. (8.1), one can easily find the wavelength shift caused by temperature change:

$$\Delta\lambda = \beta\cdot\lambda\cdot\Delta T \qquad (16)$$

For a temperature changes within a certain range, the larger the CTE of grating, the greater is the shift in central wavelength. The grating substrate employed has ultra low CTE. The CTE is zero from 0-35°C, and is less than 0.06×10^{-6}/ °C for temperature higher than 35°C (which is 1180 times less than the CTE of BK7, which is 7.1×10^{-6}/K [13]). At λ=1550nm, if temperature changes from 20 to 60°C (ΔT=40°C), the central wavelength change Δλ=0.037nm.

8.2 Insertion loss change

The change of insertion loss with temperature variation is mainly due to the change of lens focal length and vertical and lateral image shift.

8.2.1 Changes in lens focus

The thermal performance of the lens shown in Figure 6.5 was analyzed, and it was found that its focus relative to the end of the fiber mount varied with temperature. Referring to Figure 8.1, the change in back focal length Δf_b due to a change in temperature ΔT must be equal and opposite to the change in length Δz_m of the portion of the baseplate that lies between the lens and the fiber mount. That is,

$$\Delta f_b = -\Delta z_m . \tag{8.3}$$

In order to correctly calculate thermal changes in the WDDM, one must consider thermal changes in the refractive index of each lens element, the thermal expansion of the lens elements, the thermal expansion of the spacers between the optical parts, and the thermal expansion of the grating period. All of these parameters were handled by the optical design software (ZEMAX) that was used for WDM optical design, so that we were able to accurately simulate thermal changes of back focal length and overall optical performance.

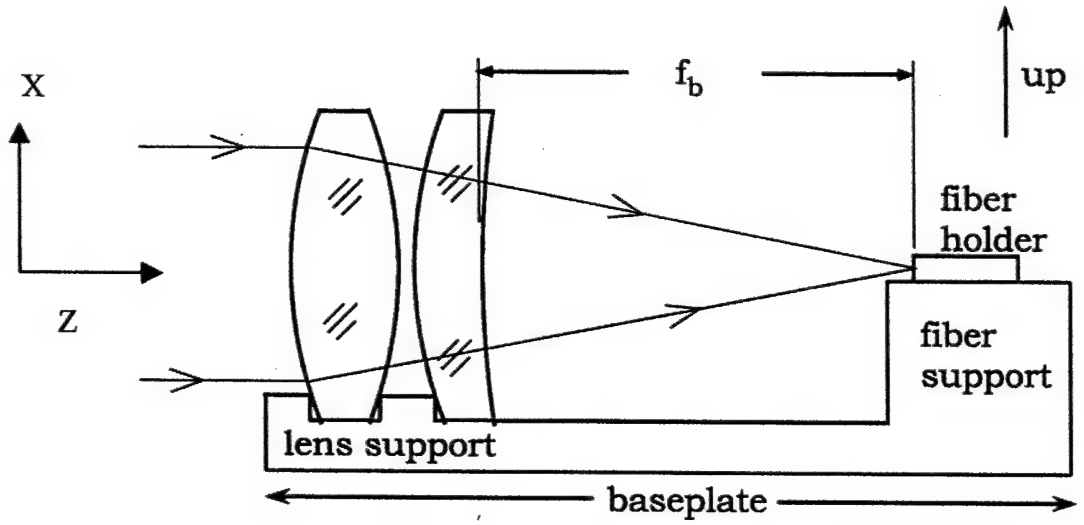

Fig. 8.1 A simplified cross-sectional view of the section of a DEMUX that includes the lens and the fiber holder.

Because available optical glasses have wide variations in the first derivative of the refractive index with respect to temperature, one is able to select a glass or glasses for the lens elements that not only will satisfy Eq.(8.3) for a chosen baseplate material, but will also provide

an opportunity for the lens to be aberration-corrected over the entire temperature range. That is, we have been able to fully optimize our lenses to have athermal performance, considering the effect of expansion in the lens spacers and the mount. This is a considerable improvement, compared to the conventional approach of merely keeping the effective focal length or the back focal length constant.

8.2.2 Image shift in vertical direction

A simplified cross sectional view of a typical diffraction grating-based DWDM is shown in Figure 8.2. The image shift in vertical direction can be expressed as:

$$\Delta x = -\tfrac{1}{2} D\Delta T(\beta_L - \beta_M). \tag{8.4}$$

Where, D is the diameter of lens, ΔT is the change of temperature, β_L and β_M are the CTE of lens and its supporting parts. Equation (8.3) indicates that, when the temperature changes within a certain range, the better matched the CTE of the lens and its supporting materials is, the less is the image shift, and therefore, the lesser is the insertion loss change.

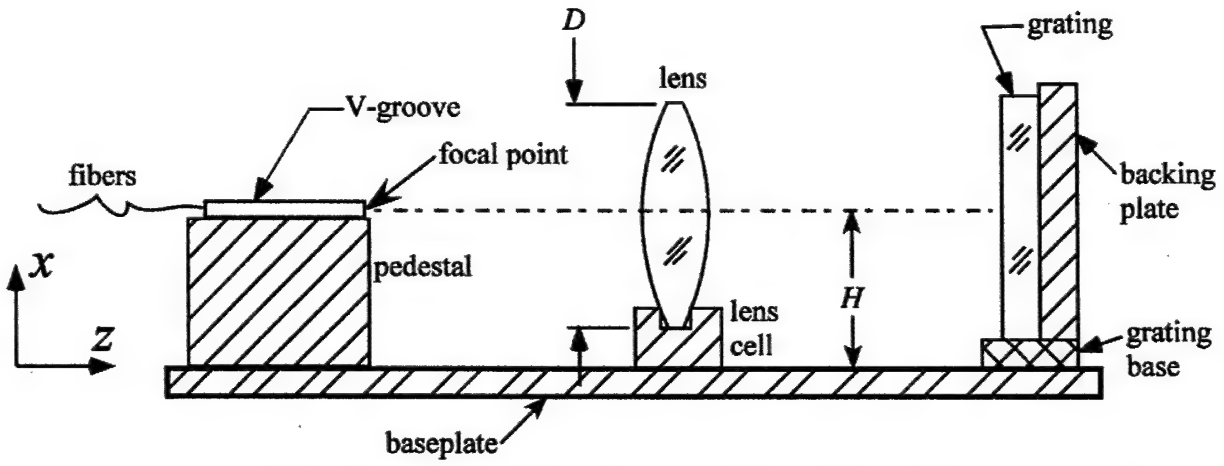

Fig. 8.2 A simplified cross sectional view of a typical grating-based DWDM. The dispersion is in the y-z direction, and the y-axis points away from the reader's eye.

The differential expansion in the vertical direction is directly proportional to the lens diameter, so that thermal problems become severe for large lenses unless the expansion coefficients of the lens elements are nearly equal to each other and to that of the support. For the dense multi-mode DWDM (D=18mm), we used stainless steel as supporting material for all the parts whose CTE is 9.9×10^{-6}/K. We chose F7 as lens material since it has almost the same CTE

(9.8×10^{-6}/K) as stainless steel. Its image shift is 0.072 μm, which can be ignored compared to the fiber core diameter (9.5 μm).

8.2.3 Image shift in dispersion direction

Because the WDM system is symmetric in lateral direction, the image shift in lateral direction is mainly caused by the change of central wavelength.

The lateral image shift Δy can be expressed as:

$$\Delta y \cong \frac{2 \cdot \Delta\lambda \cdot \tan\theta_{diff} \cdot f}{\lambda} \tag{8.5}$$

Where, Δλ is the shift of working wavelength caused by temperature variation. Combining equation (6.4) and (8.2), one can easily obtain the relation between lateral image shift and CTE of grating material and temperature change.

$$\Delta y \cong 2\beta \cdot \Delta T \cdot f \cdot \tan\theta_{diff} \tag{8.6}$$

It is obvious that the larger the diffraction angle or the larger the CTE of grating material, the greater the lateral image shift with temperature. In our design, we use ULE grating which effectively suppressed the image lateral shift to 0.12μm. It can be ignored considering the large core size of fibers.

The optical performance of the demultiplexer was diffraction-limited at all wavelengths and invariant with temperature. It is expected that this design have no observable changes in insertion loss with temperature, provided the alignment is maintained. A WDDM can give excellent performance at room temperature, but still be misaligned. This misalignment can cause significant changes in signal as the temperature changes. Thus, it may be necessary to check that, at room temperature, an alignment parameter is near the center of its range, not merely within its range.

9.0 DEVICE PACKAGING AND PERFORMANCE

A 32-channel single-mode-in and single-mode-out demultiplexer was built and tested. Figure 9.1 shows the solid mode mechanical drawing and a packaged module of this DEMUX. The entire package size is 10.5×3.0×0.9 inch. The multiplexer was fabricated as a stand-alone unit employing a stainless steel housing to provide a thermal expansion coefficient compatible with the lens material. The entire assembling and packaging process is passive and epoxy-free, which avoids the possible wavelength and insertion loss shifting caused by the UV curing of epoxy. Through improving the mechanical design, careful choices of optical materials, employing the epoxy-free packaging and sealed package housing, one expects to obtain excellent thermal behavior for this DEMUX.

The spectral passband of the 32-channel WDDM is shown in Figure 9.2 as measured using an ASE source. The average insertion loss was 4.5 dB, and the standard deviation was 0.74dB. The wavelength accuracy is within 0.078 nm. The 1dB passband varied from 0.09 to 0.16 nm, and the 3dB passband varies from 0.16 to 0.26 nm. The variation among channels was mainly due to the non-uniform spacing of the fiber array (varying from 140.1 to 164.4μm from one end to the other). The theoretical 3dB passbands varies from 0.219 to 0.257 nm. This outcome was in relatively good agreement with the experimental results. The average measured 3dB passbands (0.2 nm) were slightly smaller than the theoretical ones (0.23 nm).

Fig. 9.1 Solid model assembly drawing(left) and a packaged WDDM module (right).

This difference arises because it is quite difficult to control the exact position of the front faces of individual fibers during silicon v-groove array fabrication. In addition, polishing after fabrication might cause the length of the graded-index fiber to be smaller than designed. The passband is much better than simply using standard single-mode fibers as output fibers. The theoretical 3dB passband of 100GHz DWDM using standard single-mode fibers is only 0.06 nm.

The average crosstalk is –51dB, which is the best channel isolation so far achieved by any WDM technology. The average PDL is 0.36 dB. Table 9.1 shows the detailed measurement results for wavelength; insertion loss; passband at the 1-dB, 3-dB, and 20-dB points; crosstalk; and polarization independence loss without any serious distortion. This data rate is much higher than the 1 to 2.5 GHz rates to which our system is designed.

We also tested the data transmission bit rate of this demultiplexer. We tested the WDM module with a high-speed Bit Error Rate Tester (BERT), which was being demonstrated to us by representatives of Agilent. Figure 9.3 shows the eye diagram achieved in this quick study, which indicates that the module can process signals up to 12.5GHz

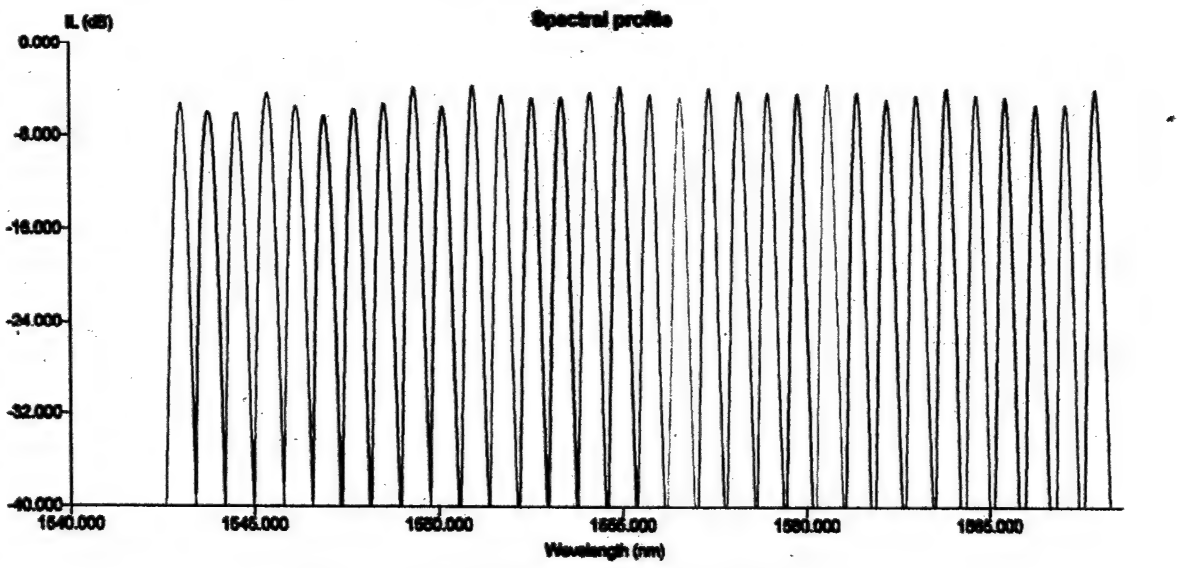

Fig. 9.2 Output spectrum of the DEMUX.

TABLE 9.1 PERFORMANCE OF THE DEMUX.

	Design Wavelength (nm)	Measured Wavelength (nm)	Difference (nm)	Insertion Loss (dB)	BW1: @ 1.00 dB (nm)	BW2: @ 3.00 dB (nm)	Crosstalk (dB)	PDL (dB)
1	1567.9522	1567.953	0.0008	3.874	0.101	0.179	49.77	0.828
2	1567.1312	1567.132	0.0008	5.099	0.093	0.164	50.09	0.821
3	1566.3138	1566.324	0.0102	5.148	0.097	0.168	48.99	0.767
4	1565.4959	1565.482	-0.0139	4.467	0.095	0.167	50.23	0.74
5	1564.6788	1564.683	0.0042	4.316	0.096	0.168	49.84	0.681
6	1563.8626	1563.881	0.0184	3.749	0.105	0.176	52.76	0.672
7	1563.0472	1563.052	0.0048	4.336	0.1	0.177	50.81	0.618
8	1562.2327	1562.244	0.0113	4.724	0.105	0.185	50.84	0.577
9	1561.4191	1561.43	0.0109	4.108	0.101	0.173	51.61	0.552
10	1560.6062	1560.627	0.0208	3.361	0.109	0.183	54.03	0.482
11	1559.7943	1559.802	0.0077	4.191	0.102	0.177	53.15	0.449
12	1558.9831	1558.981	-0.0021	4.127	0.097	0.177	52.13	0.414
13	1558.1729	1558.192	0.0191	4.053	0.108	0.188	51.71	0.378
14	1557.3634	1557.378	0.0146	3.71	0.099	0.173	54.8	0.362
15	1556.5548	1556.584	0.0292	4.487	0.099	0.172	53.78	0.313
16	1555.7471	1555.768	0.0209	4.231	0.099	0.171	53.97	0.256
17	1554.9401	1554.959	0.0189	3.61	0.109	0.19	54.89	0.269
18	1554.134	1554.146	0.012	4.059	0.113	0.199	53.2	0.197
19	1553.3288	1553.36	0.0312	4.52	0.123	0.206	50.88	0.176
20	1552.5244	1552.558	0.0336	4.552	0.11	0.193	50.79	0.13
21	1551.7208	1551.736	0.0152	4.372	0.11	0.191	52.51	0.099
22	1550.918	1550.956	0.038	3.546	0.104	0.185	51.6	0.067
23	1550.1161	1550.13	0.0139	5.357	0.123	0.216	48.95	0.013
24	1549.315	1549.357	0.042	3.703	0.119	0.206	52.03	0.068
25	1548.5148	1548.55	0.0352	5.079	0.121	0.205	48.32	0.078
26	1547.7153	1547.742	0.0267	5.554	0.123	0.211	48.12	0.096
27	1546.9167	1546.927	0.0103	6.236	0.132	0.231	49.09	0.141
28	1546.1189	1546.16	0.0411	5.288	0.133	0.223	47.22	0.186
29	1545.3219	1545.375	0.0531	4.236	0.144	0.24	49.95	0.218
30	1544.5258	1544.539	0.0132	5.909	0.135	0.235	49.07	0.26
31	1543.7305	1543.768	0.0375	5.866	0.157	0.26	46.14	0.297
32	1542.936	1543.014	0.078	5.104	0.116	0.206	46.55	0.299
Ave. (nm)			0.02055	4.5304	0.1118	0.1936	50.8694	0.36

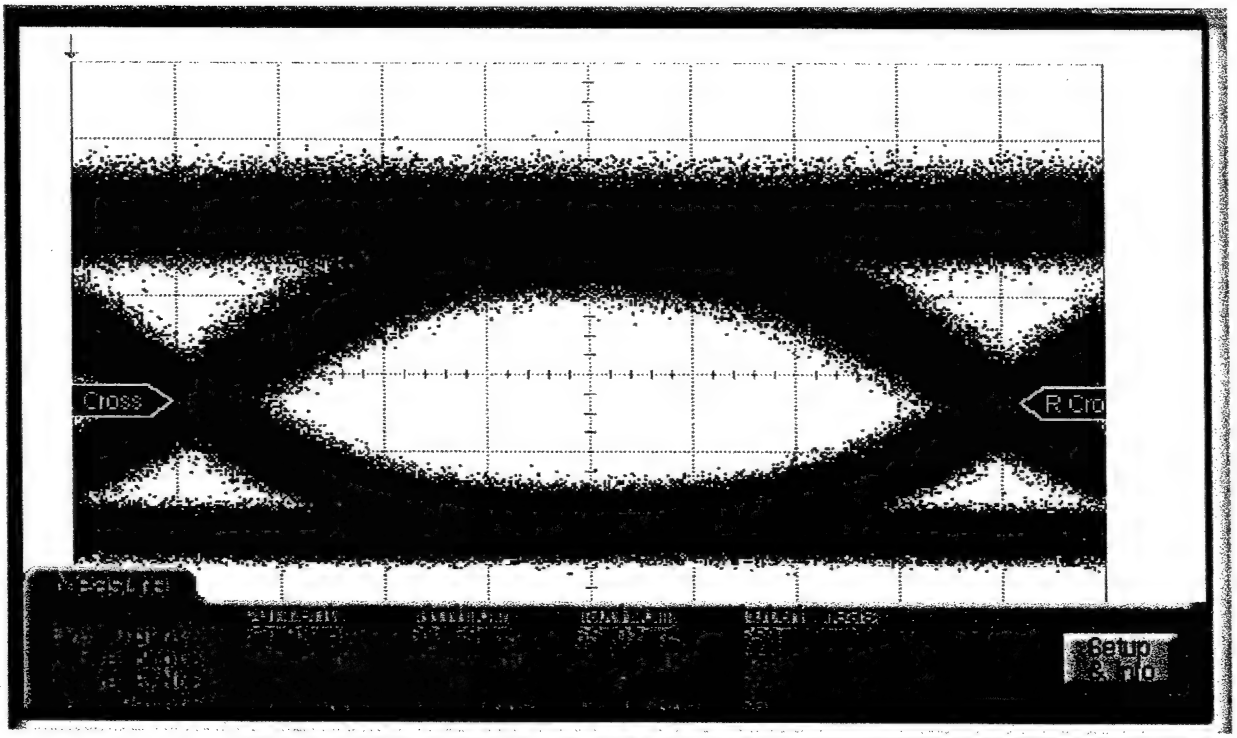

Fig. 9.3 Eye diagram of WDM device when input signal was modulate at 12.5 GHz, S/N=7.43.

10.0 INTERLEAVER FOR PASSBAND BROADENING

10.1 Interleaving technology

The employment of Interleaver technology is a solution to achieve broader passband. Basically, two separate MUX or DeMUX devices with twice the targeted channel spacing are combined to cover the entire operating window by interleaving the channels. One MUX or DeMUX covers the odd channels while the other covers the even ones (see Figure 10.1).

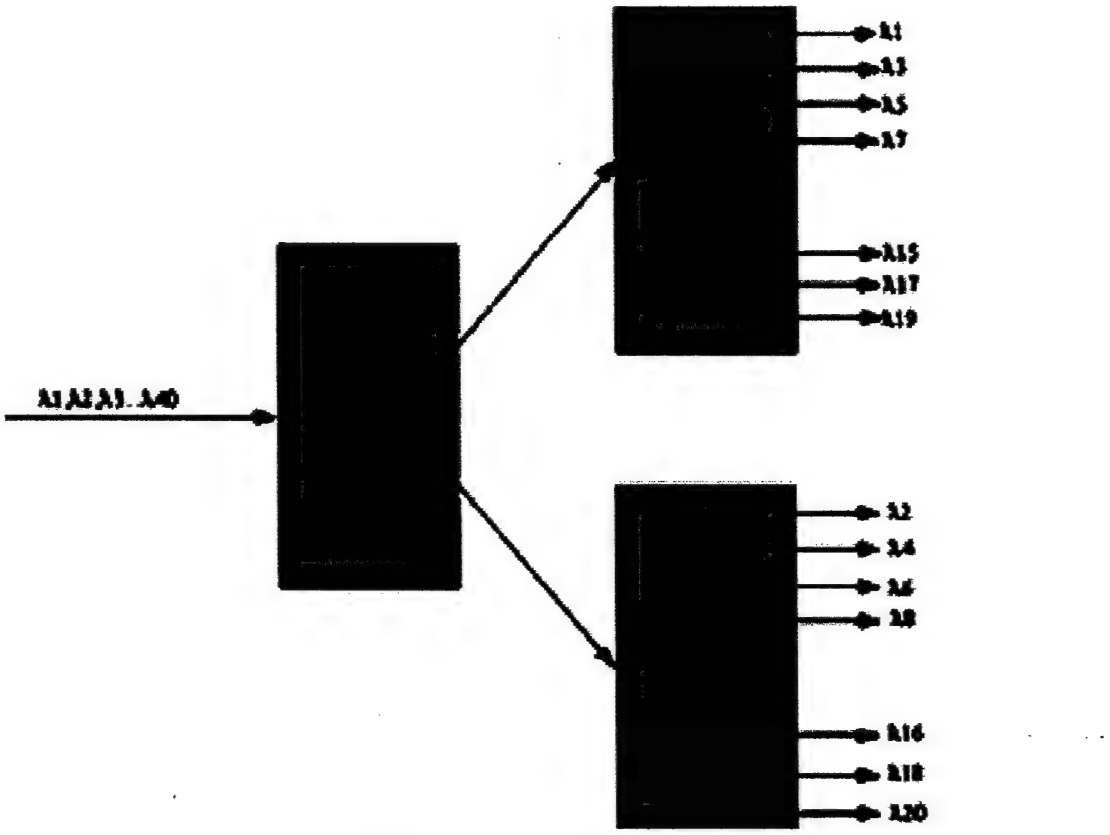

Fig. 10.1 Combination of two DeMUX devices with an interleaver performs a 100 GHz separation using two 200 GHz DeMUX components.

As is common for a new class of devices, there are a number of competing technical approaches to interleavers with no clear technical winner as of yet. The general principal behind interleavers is an interferometric overlap of two beams. The interference creates a periodic, repeating output as different integral multiples of wavelengths pass through the device, and controlling the fringe pattern sets the desired channel spacing of the device.

Manufacturers today use fused-fiber interferometers, liquid crystals, birefringent crystals and other more exotic technical approaches to build interleavers. Probably the simplest design in terms of technology and raw material is a fused-fiber, Mach-Zehnder interferometer. In this design, an unequal fiber path length between two 3-dB coupler creates the interference. By carefully controlling the path length difference, the channel spacing can be set to the desired value and matched very well to the ITU grid. Because of the all-fiber design, this technology has very low loss, uniform response over a wide wavelength range, very low dispersion and minimal polarization dependence effects. Whether as a 1 x 2 or 1 x 4 interleaver, fiber-based devices provide an excellent balance of cost, reliability, and high performance. These devices allow for extremely low insertion loss with very good isolation and bandwidth flexibility. Furthermore, very narrow channel spacings—well beyond those of today, can be achieved with an all-fiber, Mach-Zehnder device. And finally, the fiber-based devices have excellent dispersion performance, a critical feature for high bit rate systems.

Today's DWDM system deployments require a premium on performance, cost, flexibility and reliability. No single technology appears to provide the optimal solution for all applications. A careful technology selection or the application of a hybrid approach such as the pairing of interleavers and diffraction grating components can be a very attractive solution.

10.2 Optical design detail

A simplified diagram of the optics of the DEMUX is shown in Figure 10.2. Forty-channel 100GHz spaced WDM wavelengths were introduced into the DWDM device by a single-mode fiber with an FC connector, and then sent to crystal based interleaver which separated the optical signals into odd (1,3,5,...39) and even channels (2,4,6,...40).

A two-layer V-grooved fiber array was used to collect the input signals and couple the output signals. There were 21 fibers on each layer of the fiber array, in which one is used as input fiber, the other 20 fibers were used as output fibers.

The odd channels were sent to the input channel of the upper layer V-grooved fiber array. The even channels were sent to the input channel of the lower layer V-grooved fiber array. Both of the input channels were located at the far most end of the two fiber arrays. These inputs were

collimated by an optimized diffraction limited four-element lens. The same lens functions as the focusing lens for the demultiplexed signals.

Figure 10.3 shows the layout of the optics design. Because of the wide field of view in the vertical direction, one needs to used four-element lens system. We used a 1st-order echelle grating to demultiplex 40 optical signals within the C band with 100-GHz channel spacing. The working wavelength range was from 1528.37 to 1567.53 nm at the vacuum. The ITU fiber-optic telecommunications channel standard determined the wavelength choice. In order to eliminate multiple alignments for individual fibers and to increase throughput, we deployed a two-layer silicon V-grooved fiber array with 21 channel on each layer, which was designed to have variable fiber spacing because of the nonlinear effect of the angular dispersion. The each layer of the fiber array has one input single-mode fiber at one end to introduce the multiplexed signals, and has 20-single-mode output fibers to receive the 20 demultiplexed signals. The spacing of the fiber array was designed to be non-uniform varying from 32.64 to 34.72 μm to obtain accurate center wavelength within the ITU grid.

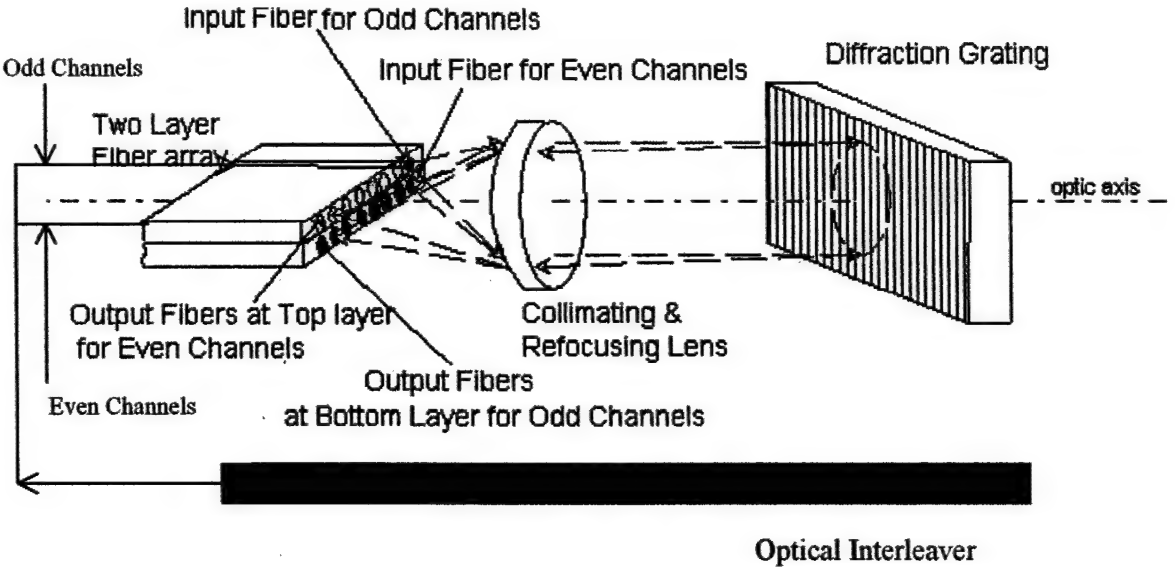

Fig. 10.2 A simplified diagram of the optics of the DeMUX using an interleaver to broaden the pass band.

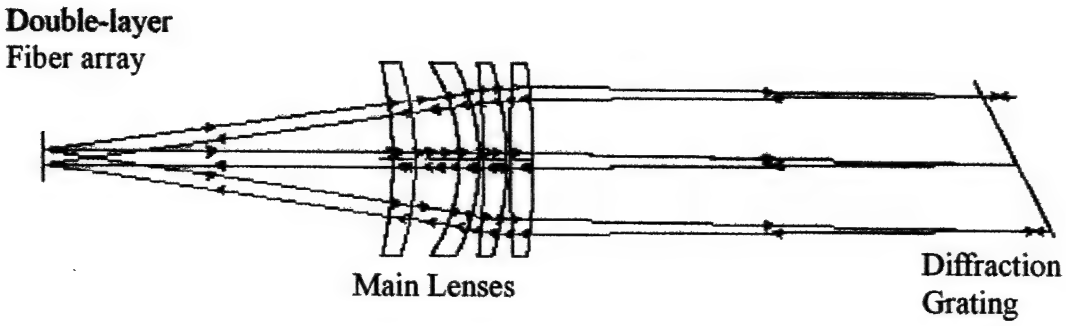

Fig. 10.3 Optical lay out of the imaging system.

In order to achieve diffraction limited optical design to obtain highest fiber coupling efficiency, we used global optimization to optimize the lens curvature, thickness, and spacing. Figure 24 shows the root mean square (RMS) of the wavefront error, which clearly shows that the RMS of wavefront error of both of the odd channels and even channels are below diffraction limit. Figure 10.5 shows the output spot diagram matrix drawing of the two-layer demultiplexer.

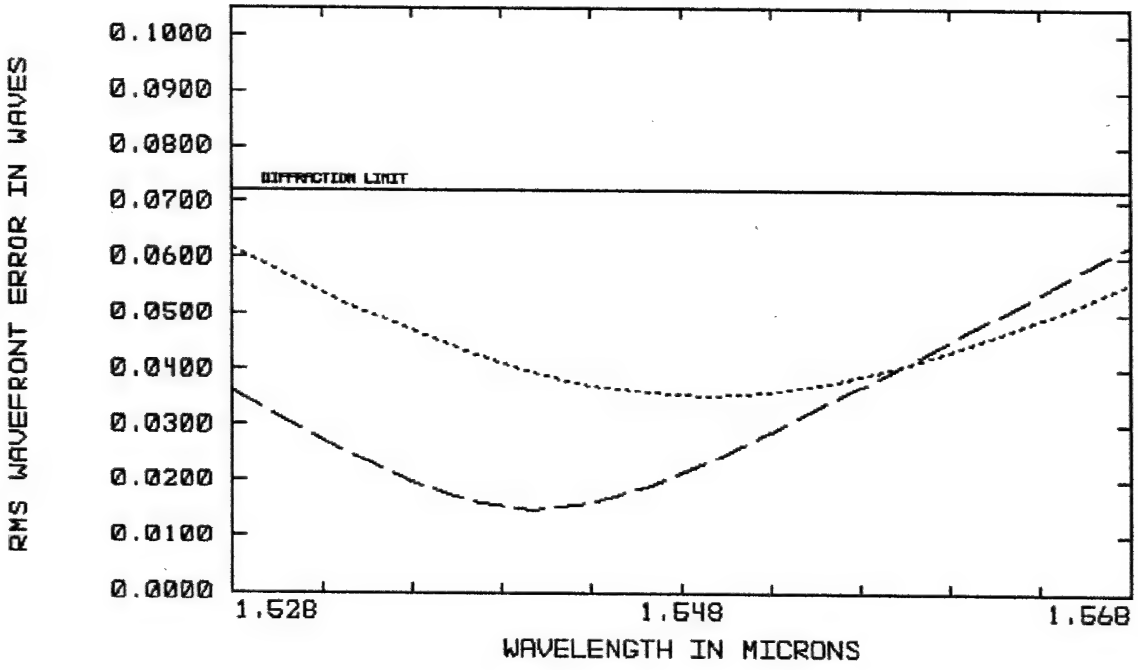

Fig. 10.4 ZEMAX simulation of root mean square wavefront error of the optics design.

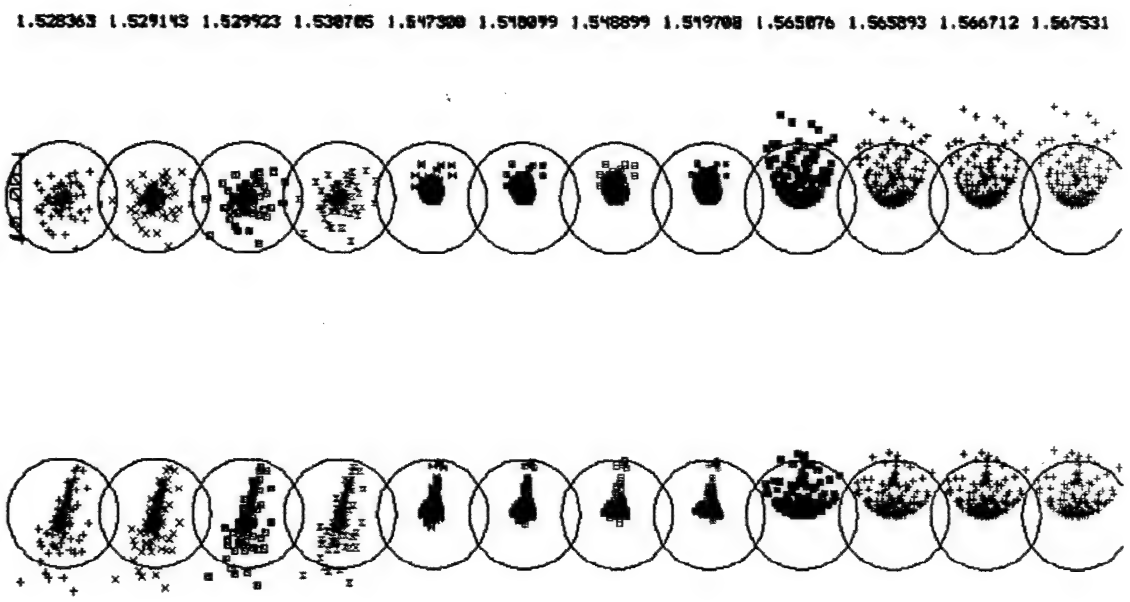

Fig. 10.5 Output spot diagram matrix drawing of the two-layer demultiplexer.

10.3 Performance of interleaver-based demultiplexer

We actually built a prototype and measured the performance of the demultiplexer. Figures 10.6, 10.7, 10.8, and 10.9 show measurement results of insertion loss, crosstalk, pass band, and polarization dependent loss, respectively

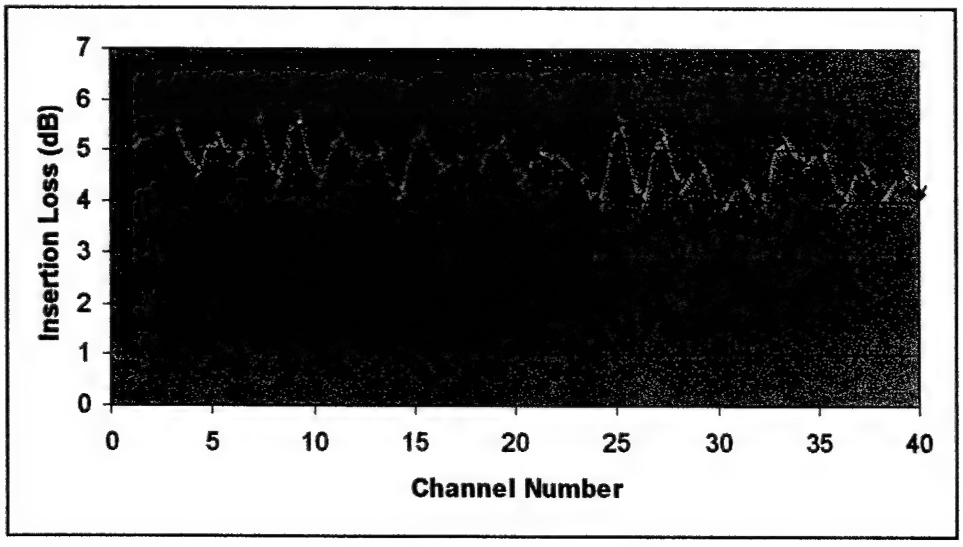

Fig. 10.6 Insertion loss measurement of the demultiplexer.

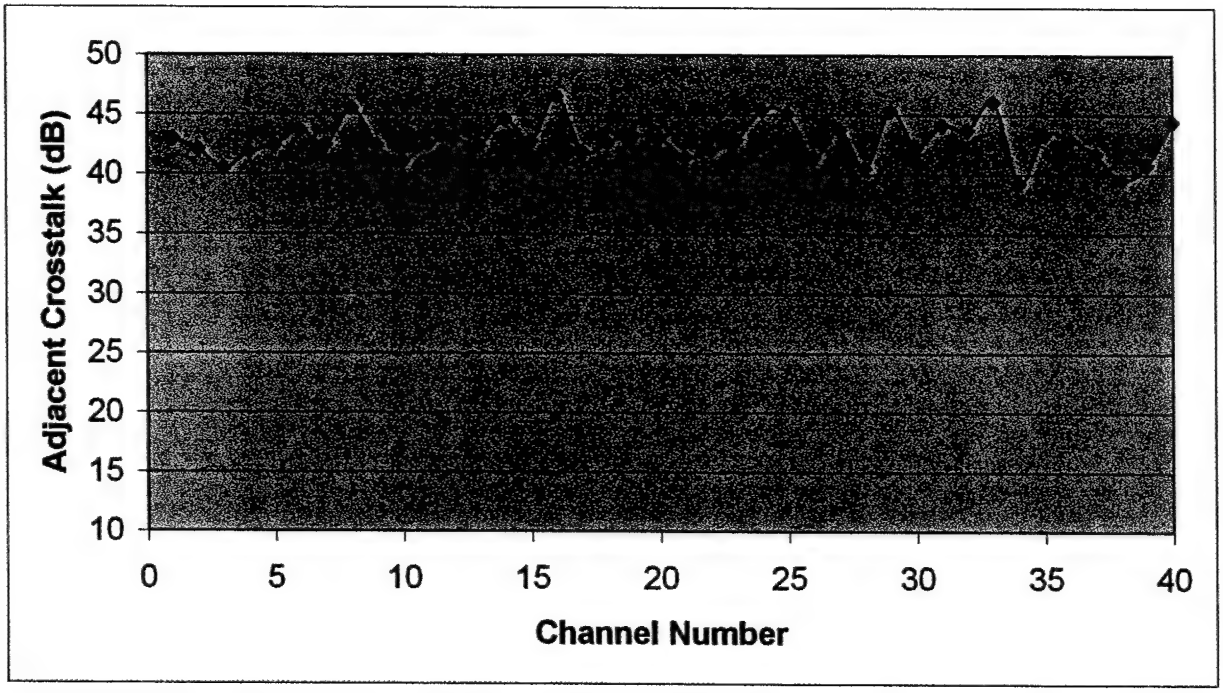

Fig. 10.7 Adjacent crosstalk measurement of the demultiplexer

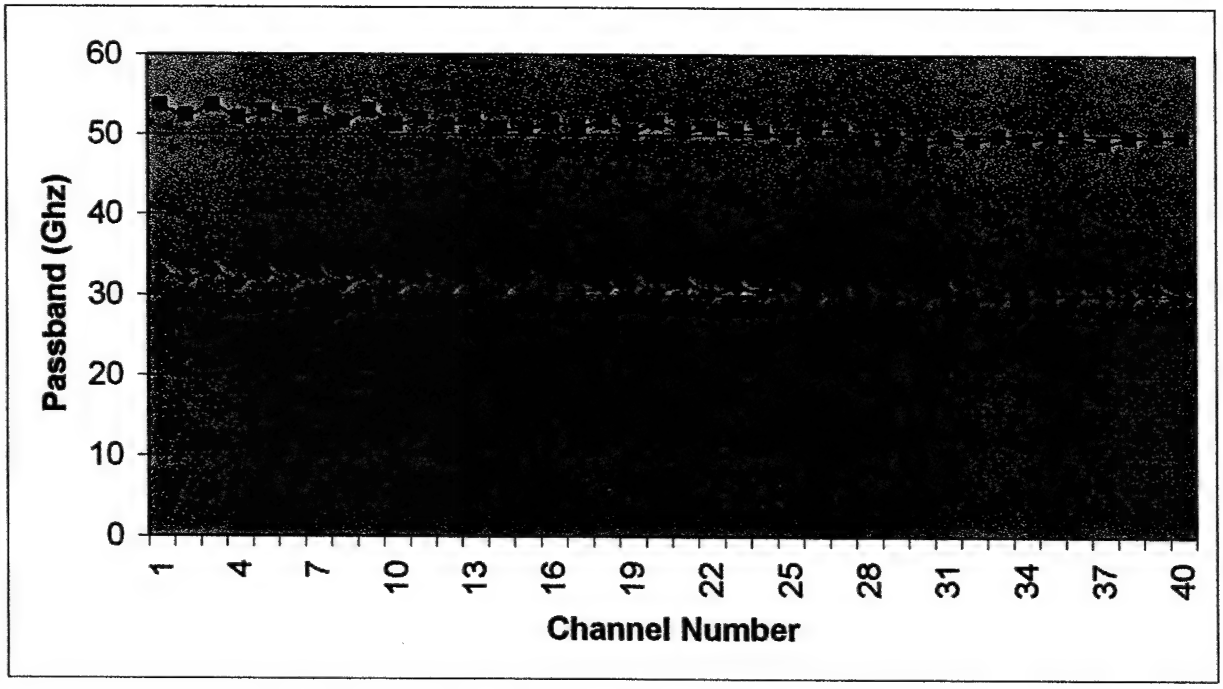

Fig. 10.8 1dB and 3dB passband of the demultiplexer

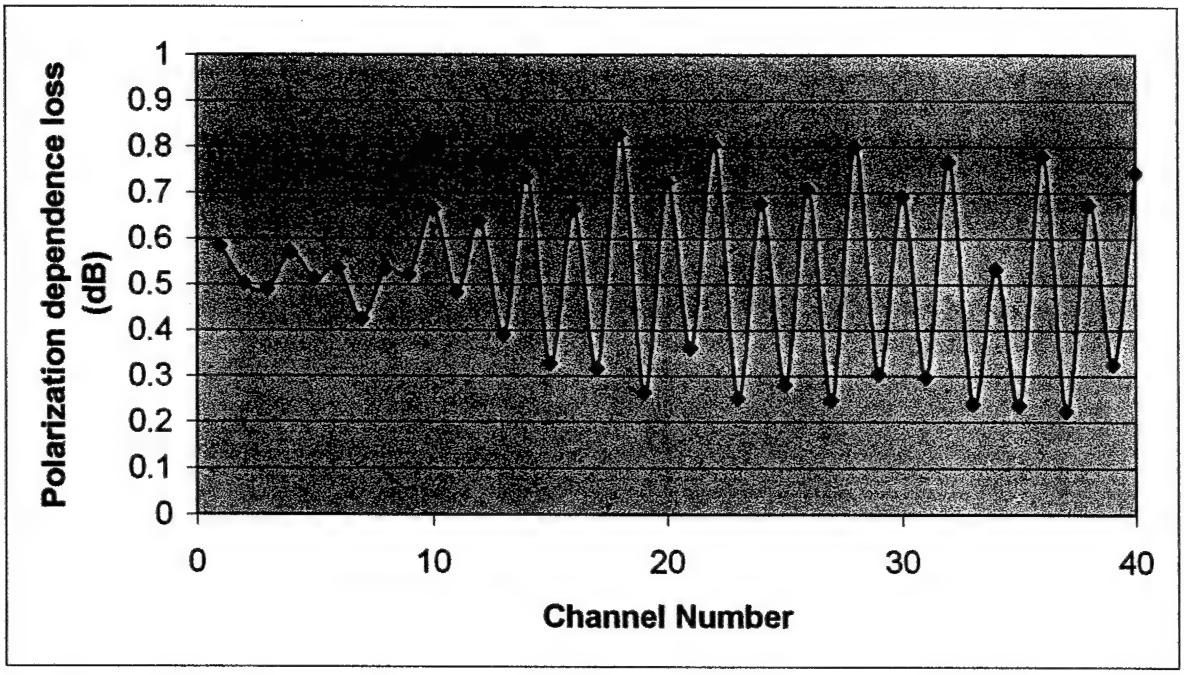

Fig. 10.9 Polarization dependent loss of the demultiplexer.

The average insertion loss of the interleaver-based demultiplexer is 4.76dB, the 1dB and 3dB passband are 31 and 51GHz respectively. Compared to the 1dB and 3dB passband without interleaver (17Ghz and 25GHz) demultiplexer, the pass band were almost doubled.

11.0 SUMMARY

In summary, this SBIR program was highly successful, and a few modules were completely packaged for delivery to the JPL labs for further testing. We contacted the JPL team at a later stage. However, it appears that JPL team was not interested in taking delivery of these modules. However, a set of 32-channel WDM/WDDM modules were successfully used to demonstrate a high throughput bit-serial data transfers between two computers for another program. The main achievements of this program are:

- The specifications, and finalized the device structure of the WDDM for bit-parallel computer architecture have been established.
- A bulk ruled reflection high-order Echelle grating was employed to realize high dispersion, to achieve high diffraction efficiency within a wide spectral range, and low polarization dependent loss. A diffraction limited triplet lens was designed to serve for both of collimation and focusing simultaneously, so the device cost and size were decreased dramatically.
- We also designed a 33-channel fiber array with non-uniform channel spacing to compensate the non-linear effect of angular dispersion.
- Graded index lensed fibers were designed and fabricated to expand the mode field diameter, and then to increase passband and alignment tolerance.
- A thorough thermal analysis and optimization has been performed to achieve athermalized WDM design and packaging.
- In order to further broaden the passband to meet the specification, a 40 channel
- 100 GHz interleaver- based DWDM were designed and a prototype was built.

The performance of the interleaver based demultiplexer was tested. The average insertion loss of the interleaver-based demultiplexer is 4.76dB, the 1dB and 3dB passband are 31 and 51GHz respectively. Compared to the 1dB and 3dB passband without interleaver (17Ghz and 25GHz) demultiplexer, the passbands were almost doubled.

12.0 REFERENCES

1. L.A. Bergman, A. J. Mendez, and L.S. Lome, "Bit-Parallel Wavelength Links for High Performance Computer Networks," in Optoelectronic Interconnects and Packaging, ed. R.T. Chen and P.S. Guilfoyle (SPIE Critical Review of Optical Science and Technology vol. CR62, SPIE Optical Engineering Press, 1996), pp. 210-226

2. L.A. Bergman and C. Yeh, "Dynamic alignment of pulses in bit-parallel wavelength links using a shepherd pulse in nonlinear fibers for massively parallel processing computer networks," presented at the Third International Conference on Massively Parallel Processing Using Optical Interconnections, Maui, Hawaii, October 27-29, 1996

3. L. A. Bergman, J. Morookian, and C. Yeh, "WDM Component Requirements for Bit-Parallel Fiber Optic Computer Networks," (unpublished, Dec. 1997)

4. Emil S. Koteles, "Integrated Planar Waveguide Demultiplexers for High Density WDM Application", *Wavelength Division Multiplexing*, Ray T. Chen, Louis S. Lome, SPIE PRESS, **CR71**, 3-32 (1999)

5. T.Mizuochi, K.Shimizu, T.Kitayama, "All-fiber add/drop multiplexing of 6 x io gbit/s using a photo-induced bragg grating filter for WDM networks," *Optical Fiber Communications*, 116 –117 (1996)

6. Hee Su Park; Seok Hyun Yun; In Kag Hwang; Sang Bae Lee; Byoung Yoon Kim, "All-fiber add-drop wavelength-division multiplexer based on intermodal coupling," *IEEE Photonics Technology Letters*, **13** (5), 460 –462 (2001)

7. M.Ibsen, R.Feced, P.Petropoulos, M.N. Zerva, "99.9% reflectivity dispersion-less square-filter fibre Bragg gratings for high speed DWDM networks," *Optical Fiber Communication Conference, 2000* , **4** , 230 -232 (2000)

8. Loren F. Stokes, "Optical-fiber filters for wavelength division multiplexing," *IEEE Circuits and Devices Magazine*, 12 (5), 49 –50 (1996).

9. F. Bilodeau, D. C. Johnson, S. Theriault, B. Malo, J. Albert, and K. O. Hill, "An all-fiber dense-wavelength-division multiplexer/demultiplexer using photoimprinted Bragg gratings," *IEEE Photon. Technol. Lett.* **7**, 388-390 (1995).

10. I. Baumann, J. Seifert, W. Nowak, and M. Sauer, "Compact all-fiber add-drop-multiplexer using fiber Bragg gratings," *IEEE Photonics Technology Letters* **8**, 1331-1333 (1996).

11. Yoshinori Hibino, "High constrast waveguide devices," *Optical Fiber Communication Conference*, Paper **WB1-1**, Anaheim, California, March 17-22, 2001

12. Y. Hida, Y. Hibino, T. Kitoh, Y. Inoue, M. Itoh. T. Shibata, A. Sugita, and A. Himeno, "400-channel 25-GHz spacing arrayed-waveguide grating covering a full range of C- and L-bands," *Optical Fiber Communication Conference*, Paper **WB2-1**, Anaheim, California, March 17-22, 2001

13. M. Oguma, T. Kitoh, K. Jinguji, T. Shibata, A. Himeno and Y. Hibino, "Flat-top and low-loss WDM filter composed of lattice-form interleave filter and arrayed-waveguide gratings on one chip," *Optical Fiber Communication Conference, 2001.* **3**. wb3-1 - wb3-3. (2001) .

14. P. D. Trinh, S.Yegnanarayanan, F.Coppinger, B.Jalali, "Silicon-on-insulator phased-array waveguide grating WDM filter," *Optical Fiber Communication Conference, OFC 97*, 301 – 302 (1997)

15. Wenhua Lin, Haifeng Li, Chen, Y.J., M. Dagenais, D. Stone, "Dual-channel-spacing phased-array waveguide grating multi/demultiplexers," *IEEE Photonics Technology Letters* , **8** (11), 1501 –1503 (1996).

16. Y. Inoue, A. Kaneko, F. Hanawa, H. Takahashi, K. Hattori, S. Sumida, "Athermal silica-based arrayed-waved-waveguide grating multiplexer," *Electronics Letters*, **33** (23), 1945-1947 (1997)

17. C. G. M. Vreeburg, *et al.*, "A low-loss 16-channel polarization dispersion-compensated PHASAR demultiplexer," *IEEE Photon. Technol. Lett.* **10**, 382-384 (1998).

18. Jie Qiao, Feng Zhao, James W. Horwitz, Ray T. Chen, "32 Channel 100GHzSpaced Demultiplexer for Metropolitan Area Network," *Optical Engineering*, **40** (7), 1255-1299 (2001)

19. Feng Zhao, Jie Qiao, Xuegong Deng, Jizuo Zou, Baoping Guo, Ray Collins, Victor Villavicencio, Kwei K. Chang, Janmes W. Horwitz, Bill Morey, Ray T. Chen, " Reliable

grating-based wavelength division (de)multiplexers for optical networks," *Optical Engineering*, **40** (7), 1204-1211 (2001)

20. George J. Cannell, Alex Robertson, Robin Worthington, "Practical realization of a high density diode-coupled wavelength demultiplexer," *IEEE Journal of selected areas in communications*, **8** (6), 1141-1145 (1990)

21. J.P. Laude, I. Long, D. Fessard, "Low loss, low crosstalk M*N passive wavelength routers based on difraction gratings ," Lasers and Electro-Optics Society Annual Meeting, 1997. *LEOS '97 10th Annual Meeting. Conference Proceedings, IEEE*, **2**, 506 -507 (1996)

22. Stamatios V. Kartalopoulos, *Introduction to DWDM technology: Data in rainbow*, Bellingham,Wash.(1999).

23. Jerry Bautista and Robert Shine, "Filter technologies vie for DWDM system applications," www.fiberopticsonline.com/content/news/article.asp

24. Telecommunication Standardization Sector of the International Telecommunication Union (ITU-T), Place des nations, CH-1211 Geneva 20, Switzerland (http://www.itu.ch).

25. McGuire and P. Bonenfant, "Standards: The blueprint for optical networking," *IEEE Commun. Mag.*, **36**, 68-75 (1998).

26. **Jie Qiao**, Feng Zhao, Jian liu, Ray T. Chen, 'Dispersion-enhanced Volume Hologram for Dense Wavelength-Division Demultiplexer' *IEEE Photonics Technology Letters*, 12 (8), 1070-1072 (2000)

27. E.G. Churin and P. Bayvel, "Pass band flattening and broadening techniques for high spectral efficiency wavelength demultiplexers," *Electronics Letters*, **35** (1), 27-28 (1999)

28. M.C. Hutley, *Diffraction Gratings*, 35, Academic Press, New York, New York (1982)

29. C. Dragone, T. Strasser, G.A. Bogert, L.W. Stulz P. Chou, "Waveguide grating router with maximally flat passband produced by spatial filtering," *Electronics Letters*, **33** (15), 1312 – 1314 (1997)

30. A.Rigny, A.Bruno, H. Sik, "Multigrating method for flattened spectral response wavelength multi/demultiplexer," *Electronics Letters*, **33** (20), 1701 –1702 (1997)

31. C.P.Botham, "Theory of tapering single-mode optical fibres by controlled core diffusion," *Electronics Letters*, **24** (4), 243-244 (1988)

32. J.S Harper, C.P.Botham; S. Hornung, "Tapers in single-mode optical fibre by controlled core diffusion," *Electronics Letters*, **24** (4), 245-246 (1988)

33. Duncan T. Moore, "Gradient-index optics: a review," *Applied Optics*, **19**(7), 1035-1043 (1980).

34. Kazou Shiraishi, Akira Ogura, and Kota Matsuura, "Spotsize contraction in standard single-mode fibers by use of a GI-fiber tip with a high focusing parameter," *IEEE Photonics Technology Letters*, **10** (12), 1757-1759 (1998)

35. W. Bludau and R. Rossberg, "Low-loss laser-to-fiber coupling with negligible optical feedback," *Journal of Lightwave Technology*, **LT-3**, 294-302 (1985)

36. Kazuo Shiraishi, "A new lensed-fiber configuration employing cascaded GI-fiber chips," *Journal of Lightwave Technology*, **18**(6), 787-794 (2000).

37. J. Laude and K. Lange, "Dense wavelength division multiplexer and routers using diffraction grating, " *Proc. of NFOEC 99*, **1**, 83-88 (1999)

38. Herwig Kogelnik, "Imaging of optical modes – resonators with internal lenses," *Bell System Technical Journal*, **44**, 455-495 (1965).

39. William L. Emkey and Curtis A. Jack, "Analysis and evaluation of graded-index fiber-lenses," *Journal of Lightwave Technology*, **LT-5** (9), 1156-1163 (1987)

13.0 CONTRIBUTING SCIENTISTS AND ENGINEERS

Dr. Jie Qiao

Dr. Feng Zhao

Dr. Xuegong Deng

Dr. Bipin Bihari

Dr. Jizuo Zou

Dr. Baoping Guo

Mr. Ray Collins,

Mr. Victor Villavicencio

Mr. Kwei K. Chang

Mr. Janmes W. Horwitz

Dr. Bill Morey

Dr. Ray T. Chen